SMALL SIGNAL STABILITY ANALYSIS OF DOUBLY FED INDUCTION OR DIRECT DRIVE SYNCHRONOUS WIND TURBINE GENERATOR INTEGRATED POWER SYSTEM

by

Faria Kamal

A thesis submitted to the faculty of
The University of North Carolina at Charlotte
in partial fulfillment of the requirements
for the degree of Master of Science in
Electrical and Computer Engineering

Charlotte

2016

Approved by:

____
Dr. Badrul Chowdhury

____
Dr. Valentina Cecchi

____
Dr. Abasifreke Ebong

©2016
Faria Kamal
ALL RIGHTS RESERVED

ABSTRACT

FARIA KAMAL. Small signal stability analysis of doubly fed induction generator or direct drive synchronous generator integrated power system. (Under the direction of DR. BADRUL CHOWDHURY)

The power system stability issues concerning the integration of wind turbine generators have been under research for quite a long time now. This study focuses on the small signal stability analysis of Doubly Fed Induction Generator (DFIG) and Direct Drive Synchronous Generator (DDSG) integrated power system. For this purpose, one synchronous generator in the IEEE 14 bus test system is first replaced by a DFIG, and then by a DDSG while the wind penetration is varied between 24-40%. PSAT, a matlab based power system analysis toolbox is used to perform small signal stability analysis, where eigenvalues give the insight of system oscillations and damping. In order to improve the damping of the Wind Turbine Generator (WTG) integrated system, Power System Stabilizers (PSS) are designed for synchronous generators. Lastly, a small disturbance is created to see the impact on both the DFIG and DDSG integrated system with and without the PSSs. The key observations include the capability of WTGs to increase system stability under certain conditions, DDSG providing better damping for a certain range of penetration, and DFIG providing stability for a larger range of wind penetration. The findings were verified using time domain analysis in PSAT, where the frequency response of the synchronous generators are observed.

ACKNOWLEDGMENTS

First and foremost, I would like to thank Dr. Badrul Chowdhury for his support as my advisor and committee chair. It was due to his belief in us that I was able to complete this task with dedication and sincerity. I thank him for allowing me to work on this thesis. I would like to thank my committee members, Dr. Valentina Cecchi and Dr. Abasifreke Ebong for their valuable time and support. I am grateful to my classmates, friends, and the research group working under Dr. Chowdhury who tried to help me out with their research whenever I needed. I thank the ECE department of UNCC; for it is due the cumulative knowledge that I have gathered from them that I can aspire to be a better human being. Thank you to all the authors mentioned in my bibliography without whose work I would be at loss.

TABLE OF CONTENTS

LIST OF FIGURES viii

LIST OF TABLES xi

CHAPTER 1: INTRODUCTION 1

1.1. Background 2

1.1.1. Power System Small Signal Stability 2

1.1.2. Wind Power Technology 3

1.1.3. Impact of Wind Power on Power System Small Signal Stability Analysis 5

1.2. Problem Statement and Rationale 7

1.3. Objective 9

CHAPTER 2: LITERATURE REVIEW 10

2.1. The Theoretical Analysis of Small Signal Stability 10

2.2. Wind Model 11

2.2.1. Wind Ramp Component 13

2.2.2. Wind Gust Component 13

2.2.3. Wind Turbulence Component 13

2.3. Wind Turbines 14

2.3.1. Doubly Fed Induction Generator (DFIG) 14

2.3.2. Direct Drive Synchronous Generator (DDSG) 21

2.4. Order of the System 25

2.4.1. Generator Order 25

2.4.2. Order of Automatic Voltage Regulator 26

2.4.3. Order of Power System Stabilizer 27

2.4.4. Order of Wind Turbine Generators 28

CHAPTER 3: METHODOLOGY 29

3.1. Small Signal Stability Analysis in PSAT 29

3.2. Power System Stabilizer Design 30

CHAPTER 4: RESULTS AND DISCUSSION 38

4.1. Base Test System 38

4.2. Case 1: DFIG Integration 42

4.2.1. Decreasing Penetration 44

4.2.2. Increasing Penetration 45

4.3. Case 2: DDSG Integration 46

4.3.1. Decreasing Penetration 46

4.3.2. Increasing Penetration 47

4.4. Case 1 vs Case 2 48

4.4.1. Lower Penetration 49

4.4.2. Higher Penetration 51

4.5. Case 3: PSS Design for DFIG Integrated System 55

4.5.1. Stability with PSS at Lower Penetration of DFIG 58

4.5.2. Stability with PSS at Higher Penetration of DFIG 58

4.6. Case 4: PSS Design for DDSG Integrated System 59

4.6.1. Stability with PSS at Lower Penetration of DDSG 62

4.6.2. Stability with PSS at Higher Penetration of DDSG 62

4.7. Comparison between Case 3 and Case 4 63

4.7.1. Lower Penetration 64

4.7.2. Higher Penetration 66

4.8. Case 5: Small Disturbance in DFIG Integrated System 68

4.8.1. Stability with Disturbance at Lower Penetration without and with the PSS 69

4.8.2. Stability with Disturbance at Higher Penetration without and with the PSS 70

4.9. Case 6: Small Disturbance in DDSG Integrated System 72

4.9.1. Stability with Disturbance at Lower Penetration without & with the PSS 72

4.9.2. Stability with Disturbance at Higher Penetration without and with the PSS 74

4.10.DFIG vs DDSG Summary 75

CHAPTER 5: CONCLUSION AND FUTURE WORK 79

5.1. Conclusion 79

5.2. Future Work 81

REFERENCES 83

APPENDIX A: POWER FLOW AND DYNAMIC DATA OF THE SYSTEM 86

APPENDIX B: CODES FOR DESIGNING POWER SYSTEM STABILIZER 88

LIST OF FIGURES

FIGURE 1: Low-pass filter to smooth wind speed variations 12

FIGURE 2: Doubly Fed Induction Generator (DFIG) 15

FIGURE 3: Rotor speed control scheme of VSWTGs 19

FIGURE 4: Voltage control scheme of VSWTGs 19

FIGURE 5: Power-speed characteristics of VSWTGs 20

FIGURE 6: Pitch angle control scheme of VSWTGs 21

FIGURE 7: Direct-Drive Synchronous Generator (DDSG) 21

FIGURE 8: Block diagram of single machine infinite bus system with exciter & AVR 31

FIGURE 9: Positive damping torque and negative synchronizing torque due to $K_2\Delta\psi_{fd}$ 34

FIGURE 10: Block diagram of single machine infinite bus system with AVR and PSS 35

FIGURE 11: Thyristor excitation system with AVR and PSS: the phase compensation, wash out and gain block 36

FIGURE 12: Test System 38

FIGURE 13: Eigenvalue plot of base case 41

FIGURE 14: Frequency vs time response of all 5 generators 41

FIGURE 15: Eigenvalue plots for 1 p.u. wind penetration 48

FIGURE 16: Generator frequency vs time plots for 1 p.u. wind penetration 49

FIGURE 17: Eigenvalue plots for 0.94 p.u. wind penetration 49

FIGURE 18: Eigenvalue plots for 0.93 p.u. wind penetration 50

FIGURE 19: Generator frequency vs time plots for 0.94 p.u. wind penetration 50

FIGURE 20: Generator frequency vs time plots for 0.93 p.u. wind penetration 51

FIGURE 21: Eigenvalue plots for 1.23 p.u. wind penetration 51

FIGURE 22: Eigenvalue plots for 1.5 p.u. wind penetration 52

FIGURE 23: Generator frequency vs time plots for 1.23 p.u. wind penetration 52

FIGURE 24: Generator frequency vs time plots for 1.5 p.u. wind penetration 53

FIGURE 25: Eigenvalue plots for 1 p.u. wind penetration 64

FIGURE 26: Generator frequency vs time plot for 1 p.u. wind penetration 64

FIGURE 27: Eigenvalue plots for decreased wind penetration 65

FIGURE 28: Eigenvalue plots for decreased wind penetration 65

FIGURE 29: Generator frequency vs time plots for decreased wind penetration 66

FIGURE 30: Generator frequency vs time plots for decreased wind penetration 66

FIGURE 31: Eigenvalue plots for increased wind penetration 67

FIGURE 32: Eigenvalue plots for increased wind penetration 67

FIGURE 33: Generator frequency vs time plots for 1.23 p.u. wind penetration 68

FIGURE 34: Generator frequency vs time plots for 1.5 p.u. wind penetration 68

FIGURE 35: Generator frequency vs time plot with small disturbance before and after adding PSS in 1 p.u. DFIG integrated system 69

FIGURE 36: Generator frequency vs time plot with small disturbance before and after adding PSS in 0.94 p.u. DFIG integrated system 70

FIGURE 37: Generator frequency vs time plot with small disturbance before and after adding PSS in 0.93 p.u. DFIG integrated system 70

FIGURE 38: Generator frequency vs time plot with small disturbance before and after adding PSS in 1.23 p.u. DFIG integrated system 71

FIGURE 39: Generator frequency vs time plot with small disturbance before and after adding PSS in 1.5 p.u. DFIG integrated system 71

FIGURE 40: Generator frequency vs time plot with small disturbance before and after adding PSS in 1 p.u. DDSG integrated system 72

FIGURE 41: Generator frequency vs time plot with small disturbance before and after adding PSS in 0.94 p.u. DDSG integrated system 73

FIGURE 42: Generator frequency vs time plot with small disturbance before and after adding PSS in 0.93 p.u. DDSG integrated system 74

FIGURE 43: Generator frequency vs time plot with small disturbance before and after adding PSS in 1.23 p.u. DDSG integrated system 74

FIGURE 44: Generator frequency vs time plot with small disturbance before and after adding PSS in 1.5 p.u. DDSG integrated system 75

LIST OF TABLES

TABLE 1: DFIG or DDSG variable introduction 15

TABLE 2: Remaining DDSG variable introduction 22

TABLE 3: Variables of exciter type II 26

TABLE 4: Variables of PSS type II 27

TABLE 5: Total generation, load and losses of the system 40

TABLE 6: Generator location before and after WTG placement 40

TABLE 7: Power flow report for 1 p.u. generation from gen. 3 40

TABLE 8: Electro-mechanical Modes of Oscillation of Base System 40

TABLE 9: Cases 42

TABLE 10: Electro-mechanical modes of oscillation after DFIG Integration at 1 p.u. 42

TABLE 11: Power flow report for decreased generation from DFIG 44

TABLE 12: Electro-mechanical modes of oscillation for decreased penetration from DFIG 44

TABLE 13: Power flow report for increased generation from DFIG 45

TABLE 14: Electro-mechanical modes of oscillation for increased penetration of DFIG 45

TABLE 15: Electro-mechanical modes of oscillation after DDSG integration at 1 p.u. 46

TABLE 16: Electro-mechanical modes of oscillation for decreased penetration of DDSG 47

TABLE 17: Electro-mechanical modes of oscillation at increased penetration of DDSG 47

TABLE 18: Electro-mechanical modes of oscillation with DFIG at 1 p.u. with PSS 58

TABLE 19: Electro-mechanical modes of oscillation after PSS design for decreased penetration from DFIG 58

TABLE 20: Electro-mechanical modes of oscillation at increased penetration from DFIG with PSS 59

TABLE 21: Electro-mechanical modes of oscillation after PSS Design with DDSG at 1 p.u. 62

TABLE 22: Electro-mechanical modes of oscillation after PSS Design with DDSG at lower penetration 62

TABLE 23: Electro-mechanical modes of oscillation after PSS Design for increased penetration from DDSG. 63

TABLE 24: Comparison between damping ratio of DFIG and DDSG integrated system without PSS at different wind penetration 76

TABLE 25: Comparison between damping ratio of DFIG and DDSG integrated system with PSS at different wind penetration 77

CHAPTER 1: INTRODUCTION

The alternative energy resources are being promoted due to their relatively benign environmental impacts and renewable nature, thereby leading to reduced dependency on traditional fossil fuels [1]. According to the Wind Vision Report, Americas current installed wind power capacity has tripled since the 2008 release of the Energy Departments 20% Wind Energy by 2030 report. It assesses the potential scenario of economic, environmental, and social benefits where wind power supplies 10% of the nations electrical demand in 2020, 20% in 2030, and 35% in 2050. Wind energy continues to thrive in the overall utility mix, with hundreds more megawatts in the pipeline [2].

As wind power becomes a significant part of a utility companys generation mix, its impact on power system stability cannot be neglected. In fact, the behavior and interaction of the generators connecting to the power system largely determines the dynamic behavior of a power system. Today, there are three major types of Wind Turbine Generators (WTGs) in the market: squirrel cage induction generators (SCIGs), doubly-fed induction generators (DFIGs) and direct-driven synchronous generators (DDSG s) or permanent magnet synchronous generator (PMSG). Due to their individual dynamic characteristics and working principles, the effects of these WTGs on power system dynamics and stability vary by large margins. Therefore, it is essential to explore the different WTGs individually [3].

1.1 Background

1.1.1 Power System Small Signal Stability

Detailed descriptions of power system small signal stability can be found in [4] and [5]. Small signal stability (or small-disturbance stability) is referred to as the ability of power system to remain in synchronism under small disturbances [4], [5]. Small signal stability problem now-a-days is often linked with the oscillatory stability problem resulting from insufficient damping torque [4], [5]. Also, two main reasons behind the lack of sufficient damping are large scale, long distance power transmission through weak AC tie lines and fast-response high-gain exciters [4]- [6]. Again, since the conventional synchronous generators would be replaced by the WTGs, it is important to note that the synchronous generator exciter and damper windings are the primary sources of internal positive damping beside loads of voltage and frequency dependency characteristics [4], [7].

In today's world, insufficient damping of oscillation contributes largely towards small signal stability. Stability of the following four types of oscillations is of concern: i) Local modes, ii) Interarea modes, iii) Control modes and iv) Torsional modes. Local modes of oscillation occur when one generating station swings with respect to the rest of the power system. Interarea modes are associated with the swinging of many machines in one part of the system against machines in other parts. Control modes are associated with with generating units and other controls where torsional modes are associated with turbine-generator shaft system rotational components. [4].

The main approaches for analyzing power system small signal stability are damping torque analysis [8], modal analysis [9], time-domain simulations [4], normal form method [10] and measurement methods based on the wide area measurement system (WAMS) [11], among which modal analysis and time-domain simulations are the two most efficient tools and they constantly complement each other [12].

The most cost effective method to introduce damping by controlling excitation systems of synchronous generators is by using power system stabilizers (PSSs). Since the conventional PSSs have limited capability to damp inter-area oscillations, different types of PSSs or damping controllers were developed to mitigate inter area oscillations and implemented in flexible AC transmission system (FACTS) [6], [13], high voltage direct current transmission (HVDC) [14], energy-storage system (ESS) [6]. The damping controllers can be local if the input signal source is local and global if the source is remote such as phasor measurement units [15].

1.1.2 Wind Power Technology

WTGs, typically consisting of a mechanical subsystem, a generator and a power electronic subsystem are used to extract the kinetic energy from the wind and then convert it into electricity. The generator subsystem and power electronics subsystem combined is called the electrical subsystem. As mentioned earlier, currently there are three kinds of WTGs in the market, among which SCIGs are the fixed or Constant Speed WTGs (CSWTGS), while DFIGs and DDSGs are Variable Speed WTGs (VSWTGs). The major discrepancies of the WTGs are the electrical subsystem and the limited aerodynamic efficiency of the wind turbine rotor of the mechanical subsystem at high wind speeds [3]. The key features of these WTGs are listed below

[3], [16]:

SCIGs-The Squirrel Cage Induction generator is connected with the wind turbine rotor through a gearbox. The stator is directly coupled to the grid with a shunt capacitor bank. A stall or active stall control is used to restrict the mechanical power extracted from the wind at high wind speeds. Despite the simplicity, robustness and low cost, the drawbacks of SCIG make the variable speed WTGs more desirable. Some of those shortcomings are: i) low energy conversion efficiency, ii) high mechanical stress, iii) gearbox maintenance requirement and iv) inability to control active and reactive power separately.

Like the SCIG, the rotor in a DFIG is connected to the generator through a gearbox and the stator is connected to the grid. However, the rotor also connects with the grid through a partial-scale converter. For restricting the mechanical power at high wind speeds, pitch control mechanism is used. DFIGs have some benefits compared to SCIGs. They are: i) maximum power point tracking (MPPT) ability by speed controller, ii) reduced mechanical stress, iii) ability to control active and reactive power independently and iv) smaller converter scale. On the other hand, DFIGs are more expensive than SCIGs and the maintenance of two gearboxes is still a requirement.

DDSGs or PMSGs- In Direct Drive Synchronous Generator or Permanent Magnet Synchronous Generator, the wind turbine rotor is directly connected to the generator and the stator is coupled to the grid through a full-scale converter. Thus, this is also called full converter synchronous generator. Like DFIGs, the mechanical power extracted from the wind can be restricted by pitch control during high wind speeds. They are similar to DFIGs to some extent such as: i) Maximum Power Point Tracking

(MPPT) ability by speed controller, ii) reduced mechanical stress, iii) flexibility to control active and reactive power. Be-sides, PMSGs can operate without gearboxes but they are heavier and incorporate converters which are larger than those for DFIGs.

1.1.3 Impact of Wind Power on Power System Small Signal Stability Analysis

A number of research efforts have taken place in recent times to address the impact of wind power on small signal stability of the power system. The wind turbine generators themselves do not take part in electromechanical oscillations as they are not synchronously connected to the grid [3], [17], [18]. Moreover, the system damping is usually affected by wind penetration through three primary mechanisms. They are: i) the electromechanical modes of the system are affected when the synchronous generators involved in electromechanical oscillations are replaced by WTGs ii) damping torques may partly be influenced if the controllers of WTGs interact with synchronous generators iii) power system damping may be influenced if the dispatch of conventional generation and profile of power flow are altered [17], [18]. The first mechanism mostly accounts for cases where conventional generation is replaced by wind generation with the system topology and power flow unchanged. While the first two mechanisms largely depend upon the type of WTGs, the last one lies independent of the wind power technology.

Among the three types, the CSWTGs do not have controllers incorporated in their electrical control for which their impact on small signal stability is not focused on as much. However, for VSWTGs, it is the other way round. Due to different dynamic characteristics, opinions on how VSWTG integration affects small signal stability vary. The two VSWTGs, i.e. DFIGs and DDSGs are supposed to have similar effects on the damping of power systems as they are partially or fully decoupled from grid, with the ability to control active and reactive power separately. What follows is a survey of the current literature on impact of WTG on small signal stability of power systems.

The issue of power system small signal stability impact of CSWTGs and VSWTGs was first initiated by J.G.Slootweg et al. in 2003 [3]. Later on, further research took place focusing this subject through modal analysis or time-domain simulations.

Generally, CSWTGs tend to contribute positively to the damping of electromechanical oscillations, because an increase in synchronous generator speed would lead to a slight voltage increase. This shifts the rotor speed versus power curve of the squirrel cage induction generator, which has a damping effect on the power system oscillation [3]- [19]. On the other hand, since the generator is decoupled from the grid by the power electronic converter in the VSWTGs, their impact on the damping cannot be generalized as such. The Nordic Grid studies by E. Hagstrom et al. show that the DFIGs and DDSGs have slightly negative impact on the inter-area oscillation damping [20].

On the contrary, O.Anaya-Lara et al. claimed DFIG's capability of improving system damping for a typical three-generator system [19], [21]. Similarly, E.Muljadi et al. showed that in a weak grid, DFIGs can exhibit good damping performance [22]. These conclusions were confirmed by G.Tsourakis et al. in [23], [24], which is an indication of the DFIG's general trend to increase inter-area oscillation damping, even though voltage control schemes may tend to reduce it. Furthermore, J.G.Slootweg et al. pointed out that the pros and cons of VSWTGs on system damping should be discussed based on oscillation types [3].

Slightly deviating from the conclusions drawn above, N .R. Ullah et al. claimed that the impact of voltage and constant power factor control mode of DDSGs on the inter-area oscillation can be beneficial or detrimental depending upon the locations of the wind farm [25]. Similarly, in [18], the analysis of eigenvalue sensitivity to inertia indicates that the DFIG integration has both positive and negative impacts on small signal stability. Again, a report by National Renewable Energy Laboratory (NREL) on Western Wind and Solar Integration Study suggests that the loss of system inertia associated with increased wind generation is of little consequence for up to at least 50% levels of instantaneous penetration for the Western Interconnection as long as adequately fast primary frequency responsive resources are maintained [26]. On a different note, it is shown that the effect of different types of WTGs on the New Zealand system damping is minimal [17].

1.2 Problem Statement and Rationale

Based on previous research, the views about the impact of VSWTGs on damping are controversial. Factors contributing towards these controversies among studies mainly include: i) types of electromechanical oscillations, ii) locations and levels of wind power penetration, iii) the system loading, and iv) different control modes of VSWTGs. Ref [3] shows that results of the analysis vary with types of oscillation modes. Also, when the synchronous generators with higher participation factors in electromechanical oscillations are replaced by VSWTGs, it might increase the damping while the replacement of others may reduce it. Secondly, the wind farms can be integrated in other appropriate locations in a way which might alter the power flow profile. Thirdly, the system loading level and penetration level of wind power play a crucial role in power system damping.

In 2014, the Minnesota utilities and transmission companies, in coordination with the Midcontinent Independent System Operator (MISO), conducted an engineering study regarding the effects on the reliability and cost of increasing Minnesotas renewable energy standard (RES) to at least 40 percent by 2030. This study assumed new wind plants were split roughly 50/50 between DFIG and DDSG. The key finding was that 40% wind and solar penetration can be reliably accommodated by the electric power system but, further analysis would be needed if it is to increase to 50% or so. Hence, this issue of "weak grid" is a relatively new area of concern within the industry. For instance, synchronous generators and condensers contribute short circuit strength to the transmission system, increasing Composite Short-Circuit Ratio (CSCR). On the other hand, Static VAR Compensators (SVCs) and Static Synchronous Compensators (STATCOMs) do not contribute towards short circuit current, and because they are electronic converter based devices with internal control systems like wind inverters, they could further reduce the effective CSCR [**?**].

Since tracking the maximum power with unity power factor is a basic active power control strategy for VSWTGs, they cannot inject oscillating power to suppress low-frequency oscillations. As a result, not so much damping contribution is expected from VSWTGs. Also, even though not as widely used, voltage or reactive power control schemes of VSWTGs have a latent impact on system damping. To conclude, due to the lack of analytical findings required, generalized conclusions cannot be provided yet [27].

This thesis, however, incorporates small signal stability analysis to compare the system stability obtained by replacing a synchronous generator with DFIG and PMSG respectively in the IEEE 14 bus test system. The impact of these two wind turbine generators on system damping varied depending on the level of wind power penetration.

1.3 Objective

The objective of this thesis is to observe the impact on small signal stability when one synchronous generator in the system is replaced by a VSWTG and the wind penetration level is varied. The eigenvalue analysis was done and the damping ratios corresponding to the participating electromechanical modes of oscillations were observed. The impact is observed first for DFIG and then for DDSG with different levels of wind power penetration. Then, in order to improve the damping, power system stabilizers for the synchronous generators were designed for both DFIG and DDSG integrated systems. Later on, a small disturbance was created in the system, and the results were compared through time domain simulations. The generator frequency responses were observed to compare the stability of DFIG and DDSG integrated system with and without power system stabilizers for various levels of wind penetration.

CHAPTER 2: LITERATURE REVIEW

2.1 The Theoretical Analysis of Small Signal Stability

The small signal stability of a power system means the ability of the system to maintain synchronism when subjected to small perturbations. As the name suggests, the disturbance is defined as a small signal in this case. Therefore, to describe the system response, the equations can be linearized by applying the linear system theory. A power system is usually described with a set of differential-algebraic equations as follows [28]:

$$x' = f(x, u) \tag{1}$$

$$y = g(x, u)$$

where system state vector x, output vector and input vector are as follows:

$$x = [x_1, x_2, x_3..., x_n]^T$$

$$y = [y_1, y_2, y_3..., y_n]^T$$

$$u = [u_1, u_2, u_3..., u_n]^T$$

f, g are linearized equations of x, u.

The f, g is linearized in the operating point to get the incremental equation:

$$\Delta\dot{x} = A\Delta x + B\Delta u \tag{2}$$

$$\Delta y = C\Delta x + D\Delta y$$

Here, A, B, C and D are the state, input, output and feedforward matrix respectively.

According to Lyapunov judgment principle of small signal stability, a system is small signal stable if all eigenvalues of the state matrix A have negative real parts.

Complex eigenvalues are conjugate, and each pair corresponds to an oscillation mode. Therefore, one pair of complex eigenvalues [28]:

$$\lambda = \delta \pm j\omega \tag{3}$$

The frequency of oscillation in Hz:

$$f = \frac{\omega}{2\pi} \tag{4}$$

Damping ratio is represented as:

$$\zeta = -\frac{-\delta}{\sqrt{\delta^2 + \omega^2}} \tag{5}$$

The damping ratio ζ determines decay rate of the oscillating amplitude. The greater the $|\zeta|$, the faster the decay [29].

2.2 Wind Model

A composite wind model which includes average speed, ramp, gust and turbulence has been used as the wind model. The first value of the wind speed sequence is the initial average speed ($v_\omega(t_0) = v_{\omega a}$) as computed at the initialization step of the wind turbines. Air density ρ at 15° and standard atmospheric pressure is $1.225kg/m^3$, and depends on the altitude (e.g. at 2000 m ρ is 20% lower than at the sea level).

Wind speed time sequences are calculated after solving the power flow and initializing wind turbine variables. During time domain simulations, the actual wind speed values which are used for calculating the mechanical power of wind turbines are the output of a low-pass filter with time constant τ. Figure 1 shows the low pass filter. In order to simulate the smoothing of high frequency wind speed variations over the

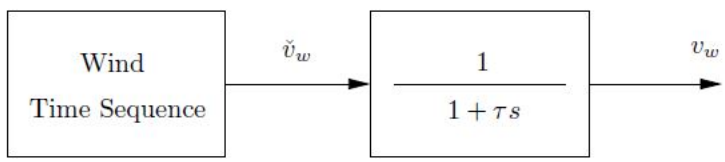

Figure 1: Low-pass filter to smooth wind speed variations [30].

rotor surface [30]:

$$\dot{v_\omega} = (\check{v_\omega}(t) - v_\omega)/\tau \tag{6}$$

The composite model considers the wind as composed of four parts, as follows:

1. average and initial wind speed $v_{\omega a}$;
2. ramp component of the wind speed $v_{\omega r}$;
3. gust component of the wind speed $v_{\omega g}$;
4. wind speed turbulence $v_{\omega t}$;

Thus the resulting wind speed $\hat{v_\omega}$ is

$$\hat{v_\omega}(t) = v_{\omega a} + v_{\omega r}(t) + +v_{\omega g}(t) + v_{\omega t}(t) \tag{7}$$

where all components are time-dependent except for the initial average speed $v_{\omega a}$.

2.2.1 Wind Ramp Component

The wind ramp component is defined by an amplitude $A_{\omega r}$ and starting and ending times, T_{sr} and T_{er} respectively:

$$t < T_{sr} : v_{\omega r}(t) = 0 \tag{8}$$

$$T_{sr} \leq t \leq T_{er} : v_{\omega r}(t) = A_{\omega r}(\frac{t - T_{sr}}{T_{er} - T_{sr}}) \tag{9}$$

$$t > T_{er} : v_{\omega r}(t) = A_{\omega r} \tag{10}$$

2.2.2 Wind Gust Component

The wind gust component is defined by an amplitude $A_{\omega g}$ and starting and ending times, T_{sg} and T_{eg} respectively:

$$t < T_{sg} : v_{\omega g}(t) = 0 \tag{11}$$

$$T_{sg} \leq t \leq T_{eg} : v_{\omega g}(t) = \frac{A_{\omega g}}{2}(1 - cos(\frac{t - T_{sg}}{T_{eg} - T_{sg}})) \tag{12}$$

$$t > T_{er} : v_{\omega g}(t) = A_{\omega g} \tag{13}$$

2.2.3 Wind Turbulence Component

The wind turbulence component is described by a power spectral density as follows:

$$S_{\omega t} = \frac{\frac{1}{ln(h/z_0)^2} l v_{\omega a}}{(1 + 1.5\frac{lf}{v_{\omega a}})^{\frac{5}{3}}} \tag{14}$$

where f is the frequency, h the wind turbine tower height, z_0 is the roughness length and l is the turbulence length scale:

$$h < 30 : l = 20h \tag{15}$$

$$h \geq 30 : l = 600 \tag{16}$$

The spectral density is then converted in a time domain cosine series as mentioned in [3]:

$$v_{\omega t}(t) = \sum_{i=1}^{n} \sqrt{S_{\omega t}(f_i)\Delta f} cos(2\pi f_i t + \phi_i + \Delta\phi) \tag{17}$$

where f_i and ϕ_i are the frequency and the initial phase of the i^{th} frequency component, being ϕ_i random phases ($\phi_i \epsilon (0, 2\pi)$). The frequency step Δf should be $\Delta f \epsilon (0.1, 0.3)$ Hz. Finally $\Delta\phi$ is a small random phase angle introduced to avoid periodicity of the turbulence signal.

2.3 Wind Turbines

This section describes the DFIG and the DDSG types as implemented in PSAT.

2.3.1 Doubly Fed Induction Generator (DFIG)

Figure 2 shows a doubly fed induction generator.

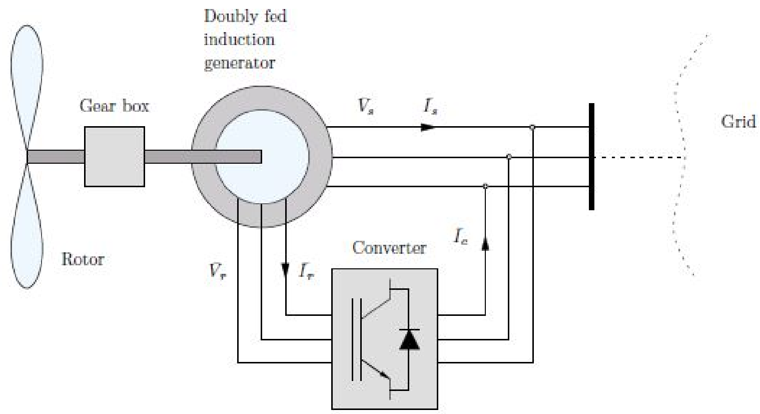

Figure 2: Doubly fed induction generator (DFIG) [30].

Table 1 introduces the variables used to describe the DFIG model. Most of them are used in DDSG as well.

Table 1: DFIG or DDSG variable introduction

Variable	**Description**	**Unit**
r_s	Stator resistance	p.u.
x_s	Stator reactance	p.u.
r_R	Rotor resistance	p.u.
x_R	Rotor reactance	p.u.
x_m	Magnetizing reactance	p.u.
H_m	Rotor inertia	kWs/kVA
K_p	Pitch control gain	-
T_p	Pitch control time constant	s
K_V	Voltage control gain	-
T_ϵ	Power control time constant	s
R	Rotor radius	m
p	Number of poles	int
η_{GB}	Gear box ratio	-
P_{max}	Maximum active power	p.u.
P_{min}	Minimum active power	p.u.
Q_{max}	Maximum reactive power	p.u.
Q_{min}	Minimum active power	p.u.

Steady-state electrical equations of the doubly fed induction generator are taken in such a way so that the stator and rotor flux dynamics are assumed much faster than the grid dynamics, and the generator is decoupled from the grid through the converter controls. These assumptions result in [30]:

$$\begin{aligned} v_{ds} =& -r_S i_{ds} + ((x_s + x_m)i_{qs} + x_m i_{qr}) \\ v_{qs} =& -r_S i_{qs} - ((x_s + x_m)i_{ds} + x_m i_{dr}) \\ v_{dr} =& -r_R i_{dr} + (1 - \omega_m)((x_R + x_m)i_{qr} + x_m i_{qs}) \\ v_{qr} =& -r_R i_{qr} - (1 - \omega_m)((x_R + x_m)i_{dr} + x_m i_{ds}) \end{aligned} \tag{18}$$

where,

v_{ds}, v_{qs}=Stator d and q axis voltage

v_{dr}, v_{qr}=Rotot d and q axis voltage

i_{ds}, i_{qs}=Stator d and q axis currents

i_{dr}, i_{qr}=Rotor d and q axis currents

The stator voltages are functions of the grid voltage magnitude V and phase θ:

$$\begin{aligned} v_{ds} =& V sin(-\theta) \\ v_{qs} =& V cos(\theta) \end{aligned} \tag{19}$$

The active and reactive powers injected into the grid depend on the stator currents and the grid side currents of the converter:

$$\begin{aligned} P =& v_{ds}i_{ds} + v_{qs}i_{qs} + v_{dc}i_{dc} + v_{qc}i_{qc} \\ Q =& v_{qs}i_{ds} - v_{ds}i_{qs} + v_{qc}i_{dc} - v_{dc}i_{qc} \end{aligned} \tag{20}$$

where i_{dc}, i_{qc} are grid side converter d and q axis currents.

The equation 20 can be rewritten considering the converter power equations, as discussed below. Firstly, the converter powers on the grid side are:

$$\begin{aligned} P_c =& v_{dc} i_{dc} + v_{qc} i_{qc} \\ Q_c =& v_{qc} i_{dc} - v_{dc} i_{qc} \end{aligned} \tag{21}$$

and, on the rotor side:

$$\begin{aligned} P_r =& v_{dr} i_{dr} + v_{qr} i_{qr} \\ Q_r =& v_{qr} i_{dr} - v_{dr} i_{qr} \end{aligned} \tag{22}$$

Secondly, assuming a lossless converter model and a unity power factor on the grid side of the converter:

$$\begin{aligned} P_c =& P_r \\ Q_c =& 0 \end{aligned} \tag{23}$$

which results into the powers injected in the grid:

$$\begin{aligned} P =& v_{ds} i_{ds} + v_{qs} i_{qs} + v_{dr} i_{dr} + v_{qr} i_{qr} \\ Q =& v_{qs} i_{ds} - v_{ds} i_{qs} \end{aligned} \tag{24}$$

As it is assumed that the converter controls are able to alter shaft dynamics, the generator motion equation is modeled as a single shaft. Thus, no tower shadow effect is considered either. Hence one has:

$$\begin{aligned} \dot{\omega_m} =& (T_m - T_e)/2H_m \\ T_e =& \psi_{ds} i_{qs} - \psi_{qs} i_{ds} \end{aligned} \tag{25}$$

where,

T_m, T_e=Mechanical and electrical torque

ψ_{ds}, ψ_{qs}=d and q axis stator fluxes

and the link between stator fluxes and generator currents is as follows:

$$\psi_{ds} = -\left((x_S + x_m)i_{ds} + x_m i_{dr}\right) \tag{26}$$

$$\psi_{qs} = -\left((x_S + x_m)i_{qs} + x_m i_{qr}\right)$$

Thus the electrical torque τ_e may be expressed as:

$$T_e = x_m(i_{qr}i_{ds} - i_{dr}i_{qs}) \tag{27}$$

The mechanical torque is:

$$T_m = \frac{P_\omega}{\omega_m} \tag{28}$$

where P_ω is the mechanical power extracted from the wind. The latter is a function of the wind speed v_ω, the rotor speed ω_m and the pitch angle θ_p. P_ω can be approximated as follows:

$$P_\omega = \frac{\rho}{2}c_p(\lambda, \theta_p)A_r v_\omega^3 \tag{29}$$

in which ρ is the air density, c_p the power coefficient or performance coefficient, λ the tip speed ratio and A_r the area swept by the rotor. The tip ratio λ is the ratio between the blade tip speed v_t and the wind upstream the rotor v_ω:

$$\lambda = \frac{v_t}{v_\omega} = \eta GB\frac{2R\omega_{\omega r}}{pv_\omega} \tag{30}$$

The $c_p(\lambda, \theta_p)$ curve is approximated as:

$$c_p = 0.22(\frac{116}{\lambda_i} - 0.4\theta_p - 5)e^{12.5/\lambda_i} \tag{31}$$

with

$$\frac{1}{\lambda_i} = \frac{1}{\lambda + 0.08\theta_p} - \frac{0.035}{\theta_p^3 + 1} \tag{32}$$

As the converter dynamics are much faster than the electromechanical transients, they are highly simplified. Therefore, the converter is modeled as an ideal current source, where i_{qr} and i_{dr} are state variables and are used for the rotor speed and voltage control respectively, which are shown in Figures 3 and Figure 4.

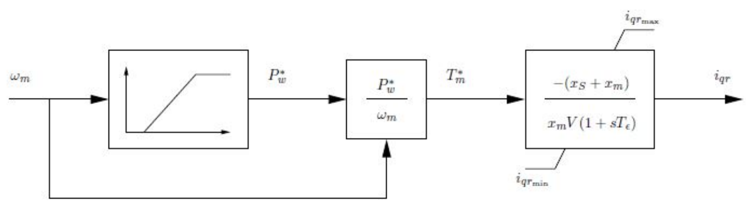

Figure 3: Rotor speed control scheme [30].

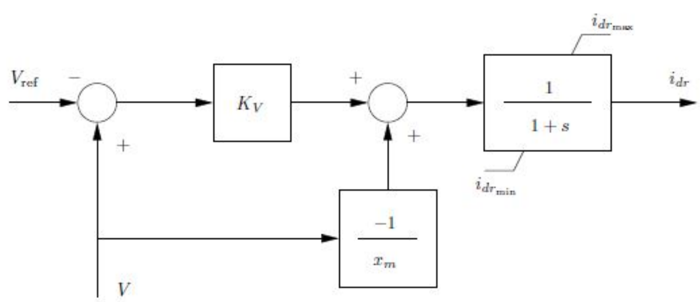

Figure 4: Voltage control scheme [30].

Differential equations for the converter currents are as follows:

$$\begin{aligned} \dot{i_{qr}} =& (-\frac{x_s + x_m}{x_m V} P_\omega^*(\omega_m)/\omega_m - i_{qr})\frac{1}{T_e} \\ \dot{i_{dr}} =& K_V(V - V_{ref}) - \frac{V}{x_m} - i_{dr} \end{aligned} \tag{33}$$

where $P_\omega^*(\omega_m)$ is the power-speed characteristic roughly optimizing the wind energy capture and is calculated using the current rotor speed value. Figure 5 shows the power-speed characteristics of VSWTGs.

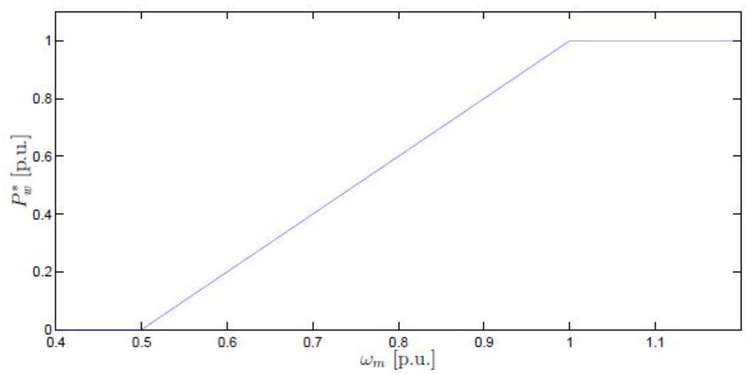

Figure 5: Power-speed characteristic [30].

It is assumed that P_ω^*=0 if $\omega < 0.5$ p.u. and that $P_\omega^* = 1$ p.u. if $\omega > 1$ p.u.

Thus, the rotor speed control only has effect for sub-synchronous speeds. Both the speed and voltage controls undergo anti-windup limiters in order to avoid converter over-currents. Current limits are approximated as follows:

$$\begin{aligned} i_{qr,max} =& -P_{min} \\ i_{qr,min} =& -P_{max} \\ i_{dr,max} =& -Q_{min} \\ i_{dr,min} =& -Q_{max} \end{aligned} \tag{34}$$

Finally the pitch angle control can be depicted in Fig. 6.

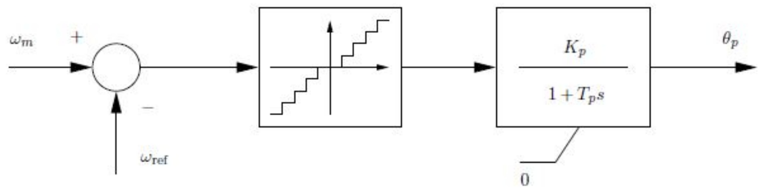

Figure 6: Pitch angle control scheme [30].

It can be expressed by the differential equation:

$$\dot{\theta}_p = (K_p \phi(\omega_m - \omega_{ref}) - \theta_p)/T_p \tag{35}$$

where ϕ is a function which allows varying the pitch angle set point only when the difference $(\omega_m - \omega_{ref})$ exceeds a predefined value $\pm\Delta\omega$.The pitch control works only for super-synchronous speeds. An anti-windup limiter locks the pitch angle to $\theta_p = 0$ for sub-synchronous speeds.

2.3.2 Direct Drive Synchronous Generator (DDSG)

Figure 7 represents a direct drive synchronous generator.

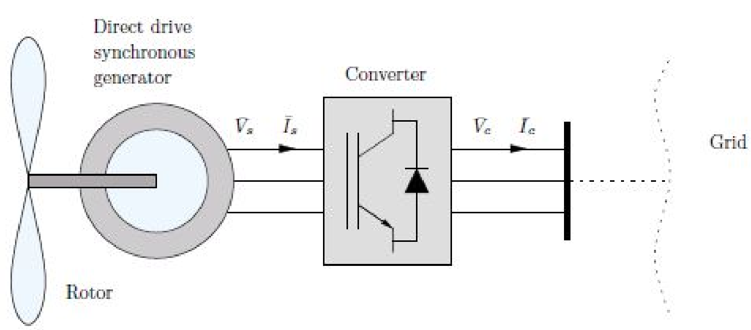

Figure 7: Direct-Drive Synchronous Generator (DDSG) [30].

Most of the variables used in DFIG model which were introduced in Table 1 are used in case of DDSG as well. The remaining ones are introduced in Table 2.

Table 2: Remaining DDSG variable introduction

Variable	**Description**	**Unit**
x_d	d-axis reactance	p.u.
x_q	q-axis reactance	p.u.
ψ_p	Permanent field flux	p.u.
T_v	Voltage control time constant	s
$T_{\epsilon p}$	Active power control time constant	s
$T_{\epsilon q}$	Reactive power control time constant	s

Steady-state electrical equations of the direct drive synchronous generator are assumed, as the stator and rotor flux dynamics are much faster in comparison with grid dynamics and the converter controls basically decouple the generator from the grid. As a result of these assumptions, one has [30]:

$$\begin{aligned} v_{ds} =& - r_s i_{ds} + \omega_m x_q i_{qs} \\ v_{qs} =& - r_s i_{qs} - \omega_m (x_d i_{ds} - \psi_p) \end{aligned} \tag{36}$$

where a permanent field flux ψ_p is used here to represent the rotor circuit. The active and reactive power of the generator are as follows:

$$\begin{aligned} P_s =& v_{ds} i_{ds} + v_{qs} i_{qs} \\ Q_s =& v_{qs} i_{ds} - v_{ds} i_{qs} \end{aligned} \tag{37}$$

while the active and reactive powers injected into the grid depend only on the grid side currents of the converter:

$$P_c = v_{dc} i_{dc} + v_{qc} i_{qc} \tag{38}$$

$$Q_c = v_{qc} i_{dc} - v_{dc} i_{qc} \tag{39}$$

where the converter voltages are functions of the grid voltage magnitude and phase, as follows:

$$\begin{aligned} v_{dc} =& V sin(-\theta) \\ v_{qc} =& V cos(\theta) \end{aligned} \tag{40}$$

Assuming a lossless converter and a power factor equal to 1, the output powers of the generator becomes:

$$P_s = P_c \tag{41}$$

$$Q_s = 0 \tag{42}$$

Moreover, the reactive power injected in the grid is controlled with the help of the converter direct current i_{dc}. Hence, equation 39 can be rewritten as follows:

$$Q_c = \frac{1}{cos(\theta)} V i_{dc} + tan(\theta) P_s \tag{43}$$

The generator motion equation is modeled as a single shaft, as it is assumed that the converter controls are able to filter shaft dynamics. For the same reason, no tower shadow effect is considered in this model. Thus one has:

$$\begin{aligned} \dot{\omega_m} =& (T_m - T_e)/2H_m \\ T_e =& \psi_{ds} i_{qs} - \psi_{qs} i_{ds} \end{aligned} \tag{44}$$

where the link between stator fluxes and generator currents is as follows:

$$\begin{aligned} \psi_{ds} =& - x_d i_{ds} + \psi_p \\ \psi_{qs} =& - x_q i_{qs} \end{aligned} \tag{45}$$

The mechanical torque and power in DDSG are modeled the same as the DFIG, thus equations from 28 to 31 apply.

Converter dynamics are highly simplified, as they are much faster with respect to the electromechanical transients. Thus, the converter is modeled as an ideal current source, where i_{qs}, i_{ds} and i_{dc} are state variables and are used for the rotor speed control, reactive power control and voltage control, respectively. Differential equations of the converter currents are given as:

$$\begin{aligned} \dot{i_{qs}} &= (i_{qsref} - i_{qs})/T_{\epsilon p} \\ \dot{i_{ds}} &= (i_{dsref} - i_{ds})/T_{\epsilon q} \\ \dot{i_{dc}} &= (K_V(V_{ref} - V) - i_{dc})/T_V \end{aligned} \tag{46}$$

where

$$\begin{aligned} i_{qsref} &= \frac{P^*_\omega(\omega_m)}{\omega_m(\psi_p - x_d i_{ds})} \\ i_{dsref} &= \frac{\psi_p}{x_d} - \sqrt{\frac{\psi_p^2}{x_d^2} - \frac{Q_{ref}}{\omega_m x_d}} \end{aligned} \tag{47}$$

Where $P^*_\omega(\omega_m)$ is the power-speed characteristic which roughly optimizes the wind energy capture and which is calculated using the current rotor speed value (Fig. 5). It is assumed that $P^*_\omega = 0$ if the $\omega_m < 0.5$ p.u. and that $P^*_\omega = 1$ p.u. if $\omega_m > 1$ p.u. Thus, the rotor speed control only has effect for sub-synchronous speeds. Both the speed and voltage controls undergo anti-windup limiters in order to avoid converter over-currents. Current limits are approximated as follows:

$$
\begin{aligned}
i_{qs,max} =& - P_{min} \\
i_{qs,min} =& - P_{max} \\
i_{ds,max} =& i_{dc,max} = -Q_{min} \\
i_{ds,min} =& i_{dc,min} = -Q_{max}
\end{aligned} \tag{48}
$$

Finally the pitch angle control is illustrated in Figure 6 and described by the differential equation 35.

2.4 Order of the System

The order of the system is the total number of state variables used in the system. These state variables are of synchronous and wind turbine generators, exciters, power system stabilizers and turbine governors etc.

2.4.1 Generator Order

Third order generators can be represented through a transfer function that has the highest exponent of three. In this model all the q-axis electromagnetic circuits are neglected, whereas a lead-lag transfer function is used for the d-axis inductance. The three state variables- angle δ, frequency ω and q-axis transient voltage $e\prime_q$ are described by the following differential equations:

$$
\begin{aligned}
\dot{\delta} =& \Omega_b(\omega - 1) \\
\dot{\omega} =& (P_m - P_e - D(\omega - 1))/M \\
\dot{e'_q} =& (-f_s(e'_q) - (x_d - x'_d)i_d + v^*_f)/T'_{d0}
\end{aligned} \tag{49}
$$

where the electrical power is:

$$P_e = (v_q + r_a i_q)i_q + (v_d + r_a i_d)i_d$$

where i_d, i_q are d and q axis current, v_d and v_q are d and q axis voltages and r_a is the armature resistance. The voltage and current link is described by the equations:

$$0 = v_q + r_a i_q - e'_q + (x'_d - x_l)i_d$$

$$0 = v_d + r_a i_d - (x_q - x_l)i_q$$

where x'_d, x_q and x_l are the d axis transient, q axis and leakage reactances. This model is the simplest one to which an automatic voltage regulator can be connected.

2.4.2 Order of Automatic Voltage Regulator

Automatic Voltage Regulators (AVRs) define the primary voltage regulation of synchronous machines. Several AVR models have been proposed and realized in practice. PSAT allows to define three simple different types of AVRs among which AVR Type II is the standard IEEE model 1. Table 3 introduces the variables used in exciter type 2 model. This can be described by the following equations:

Table 3: Variables of exciter type II

Variable	**Description**	**Unit**
v_{rmax}	Maximum regulator voltage	p.u.
v_{rmin}	Minimum regulator voltage	p.u.
K_a	Amplifier gain	p.u./p.u.
T_a	Amplifier time constant	s
K_f	Stabilizer gain	p.u./p.u.
T_f	Stabilizer time constant	s
T_e	Field circuit time constant	s
T_r	Measurement time constant	s
A_e	1^{st} ceiling coefficient	-
B_e	2^{nd} ceiling coefficient	-

$$\dot{v_m} =(V - v_m)/T_r \tag{50}$$

$$\dot{v_{r1}} =(K_a(v_{ref} - v_m - v_{r2} - \frac{K_f}{T_f}v_f) - v_{r1})/T_a$$

$$\begin{cases} v_{r1} & \text{if } v_{rmin} \leq v_{r1} \leq v_{rmax}, \\ v_{rmax} & \text{if } v_{r1} > v_{rmax}, \\ v_{rmin} & \text{if } v_{r1} < v_{rmin}, \end{cases}$$

$$\dot{v_{r2}} = -(\frac{K_f}{T_f}v_f + v_{r2})/T_f \tag{51}$$

$$\dot{v_f} = -(v_f(1 + S_e(v_f)) - v_r)/T_e$$

where the ceiling function S_e is:

$$S_e(v_f) = A_e(e^{B_e|v_f|-1})$$

This is a forth order AVR and the state variables are v_m, v_{r1}, v_{r2} and v_f

2.4.3 Order of Power System Stabilizer

Power System Stabilizers (PSSs) are typically used for damping power system oscillations and many different models are implemented in PSAT. The PSS type II adds three state variables in the system and Table 4 gives an introduction to the variables used.

Table 4: Variables of PSS type II

Variable	**Description**	**Unit**
v_{Smax}	Maximum stabilizer output signal	p.u.
v_{Smin}	Minimum stabilizer output signal	p.u.
K_ω	Stabilizer gain	p.u./p.u.
T_ω	Wash-out time constant	s
T_1	First stabilizer time constant	s
T_2	Second stabilizer time constant	s
T_3	Third stabilizer time constant	s
T_4	Fourth stabilizer time constant	s

This can be described by the equations:

$$\begin{aligned}
\dot{v_1} =& -(K_\omega v_{SI} + v_1)/T_\omega \\
\dot{v_2} =& ((1 - \frac{T_1}{T_2})(K_\omega v_{SI} + v_1) - v_2)/T_2 \\
\dot{v_3} =& ((1 - \frac{T_3}{T_4})(v_2 + (\frac{T_1}{T_2}(K_\omega v_{SI} + v_1))) - v_3)/T_4 \dot{v_s} = \quad (v_3 + \frac{T_3}{T_4}(v_2 + \frac{T_1}{T_2}(K_\omega v_{SI} + v_1)) - v_s)/T_\epsilon
\end{aligned} \tag{52}$$

the output signal V_s is subjected to an anti-windup limiter and its dynamic is given by a small time constant $T_\epsilon = 0.001\ s^2$.

2.4.4 Order of Wind Turbine Generators

The DFIG and DDSG each add 5 state variables to the system. For DFIG, they are wind speed v_ω, rotor speed ω_m, rotor q axis current i_{qr}, rotor d axis current i_{dr} and pitch angle θ_p expressed by equations 7, 25, 33 and 35.

For DDSG, the five state variables are the wind speed v_ω, rotor speed ω_m, stator q axis current i_{qs}, converter d axis current i_{dc} and pitch angle θ_p expressed by equations 7, 25, 46 and 35.

CHAPTER 3: METHODOLOGY

All simulations were carried out in Power System Analysis Toolbox (PSAT) [31], an open source MATLAB and GNU/Octave-based software package for analysis and design of small to medium size electric power system.

3.1 Small Signal Stability Analysis in PSAT

It is possible to compute and plot the eigenvalues and the participation factors of the system in PSAT, once the power flow is solved. The eigenvalues can be computed for the state matrix of the dynamic system, and for the power flow Jacobian matrix (QV sensitivity analysis) [32]. In PSAT, eigenvalues are computed using analytical Jacobian matrices, which ensures high-precision results [31].

1) Dynamic Analysis: The Jacobian matrix A_c of a dynamic system is defined by:

$$\begin{bmatrix} \Delta\dot{x} \\ 0 \end{bmatrix} = \begin{bmatrix} F_x & F_y \\ G_x & J_{LFV} \end{bmatrix} \begin{bmatrix} \Delta x \\ \Delta y \end{bmatrix} = [A_c] \begin{bmatrix} \Delta x \\ \Delta y \end{bmatrix} \tag{53}$$

where $F_x = \nabla_x f, F_y = \nabla_y f, G_x = \nabla_x g$ and $J_{LFV} = \nabla_y g$. Then the state matrix A_s is obtained by eliminating Δy, and thus implicitly assuming that J_{LFV} is nonsingular:

$$A_s = F_x - F_y J_{LFV}^{-1} G_x \tag{54}$$

With a high dynamic order of the system, the computation of all eigenvalues can be lengthy. To overcome this issue, PSAT gives the option of computing a reduced number of eigenvalues based on sparse matrix properties and eigenvalue relative values. Also, PSAT uses right and left eigenvector matrices to calculate participation factors [33].

2) QV Sensitivity Analysis: The QV sensitivity analysis is done on a reduced matrix. Assuming the power flow Jacobian matrix J_{LFV} can be divided into four sub-matrices:

$$J_{LFV} = \begin{bmatrix} J_{P\theta} & J_{PV} \\ J_{Q\theta} & J_{QV} \end{bmatrix} \tag{55}$$

The reduced matrix used for QV sensitivity analysis is defined as follows:

$$J_{LFVr} = J_{QV} - J_{Q\theta} J_{P\theta}^{-1} J_{PV} \tag{56}$$

where it is assumed that $J_{P\theta}$ is nonsingular [32]. It is to note that the Jacobian matrix used in PSAT for power flow, takes into account all static and dynamic components such as tap changer models.

3.2 Power System Stabilizer Design

The complete state-space model for the power system, including the excitation system, has the form [4]:

$$\begin{bmatrix} \Delta\dot{\omega}_r \\ \Delta\dot{\delta} \\ \Delta\dot{\psi}_{fd} \\ \Delta\dot{v}_1 \end{bmatrix} = \begin{bmatrix} a_{11} & a_{12} & a_{13} & 0 \\ a_{21} & 0 & 0 & 0 \\ 0 & a_{32} & a_{33} & a_{34} \\ 0 & a_{42} & a_{43} & a_{44} \end{bmatrix} \begin{bmatrix} \Delta\omega_r \\ \Delta\delta \\ \Delta\psi_{fd} \\ \Delta v_1 \end{bmatrix} + \begin{bmatrix} b_1 \\ 0 \\ 0 \\ 0 \end{bmatrix} \Delta T_m \tag{57}$$

where the state variables are:

$\Delta\omega_r$= speed deviation in pu = $(\omega_r - \omega_0)/\omega_0$

$\Delta\delta$= rotor angle deviation in elec. rad

$\Delta\psi_{fd}$= Field flux linkage deviation

Δv_1=Exciter voltage deviation

Figure 8 shows the block diagram representation of the excited model.

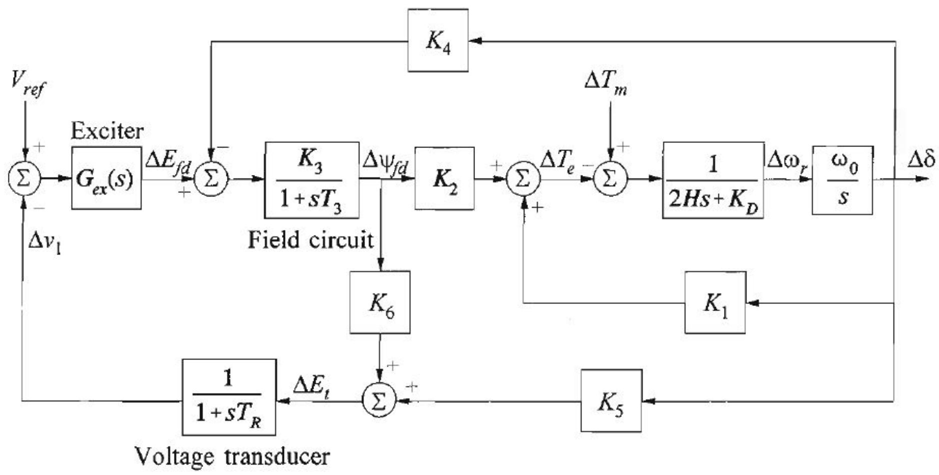

Figure 8: Block diagram representation with exciter & AVR [4].

It is applicable to any type of exciter, with $G_{ex}(s)$ representing the transfer function of the AVR and exciter. For a thyristor exciter: $G_{ex}(s) = K_A$.

$$a_{11} = -\frac{K_D}{2H} \tag{58}$$

$$a_{12} = -\frac{K_1}{2H} \tag{59}$$

$$a_{13} = - -\frac{K_2}{2H} \tag{60}$$

$$a_{21} = \omega_0 = 2\pi f_0 \tag{61}$$

$$a_{32} = -\frac{\omega_0 R_{fd}}{L_{fd}} m_1 L'_{ads} \tag{62}$$

$$a_{33} = -\frac{\omega_0 R_{fd}}{L_{fd}}[1 - \frac{L'_{ads}}{L_{fd}} + m_2 L'_{ads}] \tag{63}$$

$$b_{11} = \frac{1}{2H} \tag{64}$$

$$b_{32} = \frac{\omega_0 R_{fd}}{L_{adu}} \tag{65}$$

$$K_3 = -\frac{b_{32}}{a_{33}} \tag{66}$$

$$K_4 = -\frac{a_{32}}{b_{32}} \tag{67}$$

$$T_3 = -\frac{1}{a_{33}} = K_3 T'_{d0} \frac{L_{adu}}{L_{ffd}} \tag{68}$$

$$a_{41} = 0 \tag{69}$$

$$a_{42} = \frac{K_5}{T_R} \tag{70}$$

$$a_{43} = \frac{K_6}{T_R} \tag{71}$$

$$a_{44} = -\frac{1}{T_R} \tag{72}$$

where,

H = inertia constant in MW.s/MVA

K_D = damping torque coefficient in pu torque/pu speed deviation

$\omega_0 = 2\pi f_0 = 377$ for a 60 Hz system

L_{fd} = field inductance = $\frac{(L_{dd} * L_d)}{L_d - L_{dd}}$

R_{fd} = field resistance = $\frac{(L_d + L_{fd})}{T_{dd} a_{21}}$

T_R = terminal voltage transducer time constant

The synchronous generator parameters L_{adu} and L'_{ads} are the transient and sub-transient inductances unsaturated and saturated. The elements of the A matrix are obtained from PSAT which allows the calculation for all the gain constants K values.

With automatic voltage regulator action, the field flux variations are caused by the field voltage variations, in addition to the armature reaction. From the block diagram of Figure 8, it can be seen that:

$$\Delta\psi_{fd} = \frac{K_3}{1 + sT_3}[-K_4\Delta\delta - \frac{G_{ex}(s)}{1 + sT_R}(K_5\Delta\delta + K_6\Delta\psi_{fd})] \tag{73}$$

By grouping terms involving $\Delta\psi_{fd}$ and rearranging,

$$\Delta\psi_{fd} = \frac{-K_3[K_4(1 + sT_R) + K_5 G_{ex}(s)]}{s^2 T_3 T_R + s(T_3 + T_R) + 1 + K_3 K_6 G_{ex}(s)}\Delta\delta \tag{74}$$

The change in air-gap torque due to change in field flux linkage is:

$$\Delta T_e \mid_{\Delta\psi_{fd}} = K_2 \Delta\psi_{fd} \tag{75}$$

Figure 9 shows the damping torque and synchronizing torque resulting from $K_2\Delta\psi_{fd}$. K_1-K_6 are gain constants The effect of AVR is to increase the synchronizing torque component and decrease the damping torque component when K_5 is negative and vice versa. It will be obtained in the form $\Delta T_e \mid_{\Delta\psi_{fd}} = K_{S(\Delta\psi_{fd})} \pm K_{D(\Delta\psi_{fd})} = A\Delta\delta \pm B(j\Delta\delta)$.

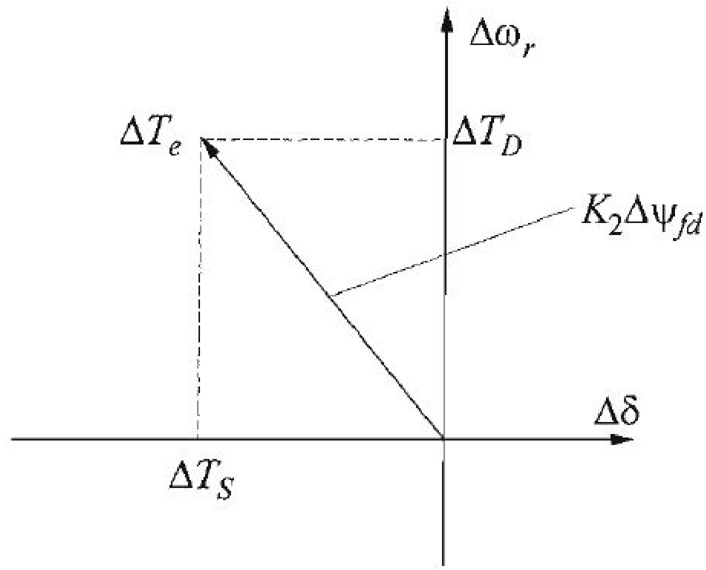

Figure 9: Positive damping torque and negative synchronizing torque due to $K_2\Delta\psi_{fd}$ [4].

Hence, the net synchronizing torque coefficient is:

$$K_s = K_1 + K_{s(\Delta\psi_{fd})} \tag{76}$$

The damping torque component due to $\Delta\psi_{fd}$ is:

$$K_{D(\Delta\psi_{fd})} = B(j\Delta\delta) \tag{77}$$

Since $\Delta\omega_r = s\Delta\delta/\omega_0 = j\omega\Delta\delta/\omega_0$,

$$K_{D(\Delta\psi_{fd})} = -\frac{B\omega_0}{\omega}\Delta\omega_r \tag{78}$$

Figure 10 shows the block diagram representation of a single bus infinite bus system with AVR and PSS.

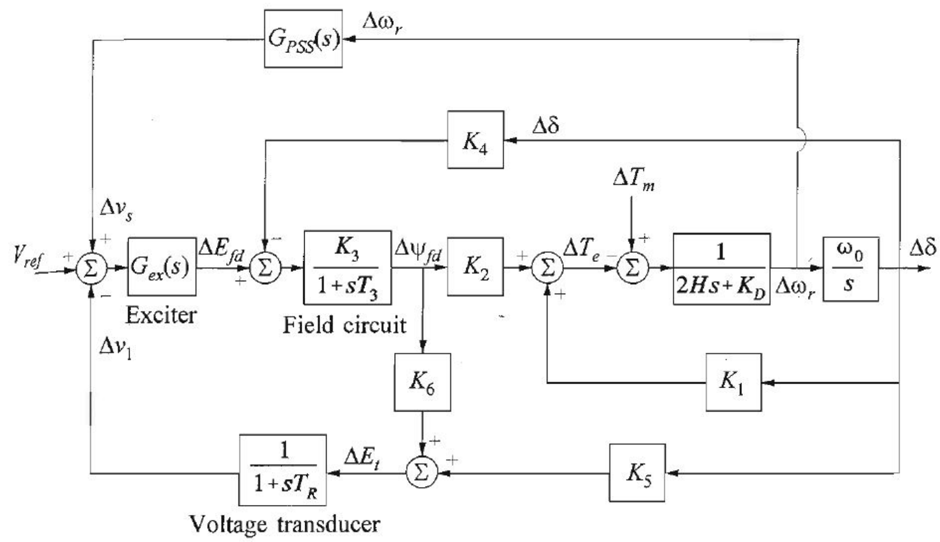

Figure 10: Block diagram representation with AVR and PSS [4]

.

From the block diagram of Figure 10, with T_R neglected (since it is very small compared to T_3), $\Delta\psi_{fd}$ due to PSS is given by:

$$\Delta\psi_{fd} = \frac{K_3 K_A}{1 + sT_3}(-K_6\Delta\psi_{fd} + \Delta v_s) \tag{79}$$

Therefore,

$$\frac{\Delta\psi_{fd}}{\Delta v_s} = \frac{K_3 K_A}{sT_3 + 1 + K_3 K_6 K_A} \tag{80}$$

Again, $\Delta T_{pss} = \Delta T_e$ due to PSS $= K_2(\Delta\psi_{fd} duetoPSS)$

Hence,

$$\frac{\Delta T_{pss}}{\Delta v_s} = k_2(\frac{\Delta\psi_{fd}}{\Delta v_s}) \tag{81}$$

which is obtained in the form $C\angle D°$. If ΔT_{pss} has to be in phase with $\Delta\omega_r$, the $\Delta\omega_r$ signal should be processed through a phase-lead network so that the signal is advanced by $\theta = D^{\circ}$ at the frequency of oscillation. The amount of damping introduced depends on the gain of PSS transfer function at that frequency. Therefore, ΔT_{pss}=(gain of PSS at the frequency of oscillation)(C)($\Delta\omega_r$).

With the phase-lead network compensating exactly for the phase lag between ΔT_e and Δv_s, the above compensation is purely damping. The damping torque coefficient due to PSS at the frequency of oscillation is equal to:

$$K_d(PSS) = (gainofPSS)(C) \tag{82}$$

Figure 11 represents the thyristor excitation system with AVR and PSS.

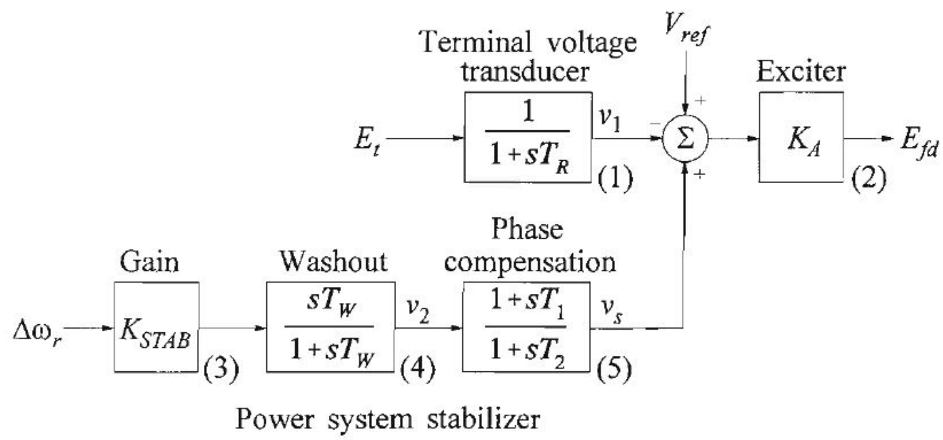

Figure 11: Thyristor excitation system with AVR & PSS [4].

The PSS representation in Figure 11 consists of three blocks: a phase compensation block, a single wash out block, and a gain block. The phase compensation block provides the appropriate phase lead characteristic to compensate for the phase lag between the exciter input and the generator electrical torque. If the angle needed to be compensated it more than 45°, two first order blocks are needed.

$$arg((1 + sT_1) - (1 + sT_2)) = \angle D^\circ \tag{83}$$

CHAPTER 4: RESULTS AND DISCUSSION

4.1 Base Test System

Figure 12 represents a one-line diagram of the well-known IEEE-14 bus test system [34]. Appendix A contains the data used to conduct a power flow and dynamic analysis of the system.

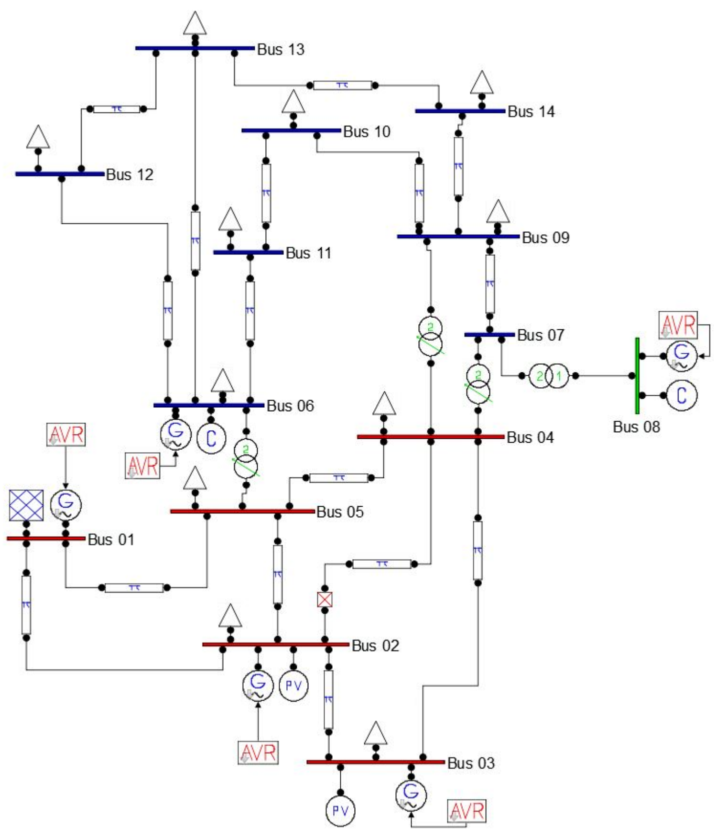

Figure 12: Modified IEEE 14 bus test system.

The system has a base of 100MVA and an order of 35 as it incorporates 5 third order (equation 49) synchronous generators and 5 fourth order (equation 50) automatic voltage regulators (AVRs).

The 100 MVA generator at bus 3 of the IEEE 14 bus test system is replaced first by a 100 MW DFIG wind farm and then by a 100 MW DDSG wind farm. On another note, after one synchronous generator with AVR is replaced by a fifth order WTG, it becomes a 33 order system. Third order (equation 51) PSSs for 3 synchronous generators are designed after the WTG is integrated, making it a 42 order system.

Originally the system is marginally stable, not asymptotically stable. This means, when the initial condition is slightly changed from equilibrium to some point near it, two things might happen: for asymptotically stable equilibrium, "displaced" motion will get back to equilibrium and, for marginal stable equilibrium, the motion will be near the equilibrium, but won't get back to it. However, after WTG integration, the stability is analyzed again. Then PSSs are designed to damp the oscillations. At last, a small disturbance is created in the system to check the stability of the system. The disturbance is a three phase fault occurring at bus 12, shedding 2.3% load of the system for 0.25 seconds.

The total real and reactive power generation, load and losses of the system are shown in Table 5. The generator numbers and where they are placed before and after the WTG integration are presented in Table 6. It also shows which of the generators are connected in PV buses supplying real power, and which generators are static synchronous compensator connected supplying only reactive power. The power flow results of the base system can be seen from Table 7. Generation from bus 3 is kept at 1 p.u. i.e. 27%:

Table 5: Total generation, load and losses of the system

Total P Generation	3.766
Total Q Generation	1.491
Total P Load	3.626
Total Q Load	1.140
Total P Losses	0.140
Total Q Losses	0.352

Table 6: Generator location before and after WTG placement

Bus No	Gen No. (Before)	Gen no. (After)
01 (Slack)	1	1
02	2	2
03	3	WTG
08	4	3
06	5	4

Table 7: Power flow report for 1 p.u. generation from gen. 3

Bus	**V**	**phase**	**P gen**	**Q gen**	**P load**	**Q load**
1	1.06	0.00	2.37	-0.13	0.00	0.00
2	1.05	-0.09	0.40	0.40	0.30	0.18
3	1.05	-0.18	1.00	0.52	1.32	0.27
4	1.01	-0.19	0.00	0.00	0.67	0.06
5	1.01	-0.17	0.00	0.00	0.11	0.02
6	1.07	-0.30	0.00	0.39	0.16	0.11
7	1.04	-0.27	0.00	0.00	0.00	0.00
8	1.09	-0.27	0.00	0.30	0.00	0.00
9	1.02	-0.31	0.00	0.00	0.41	0.23
10	1.02	-0.31	0.00	0.00	0.13	0.08
11	1.04	-0.31	0.00	0.00	0.05	0.03
12	1.05	-0.32	0.00	0.00	0.09	0.02
13	1.04	-0.32	0.00	0.00	0.19	0.08
14	1.00	-0.34	0.00	0.00	0.21	0.07

The eigenvalues are plotted in Figure 13 and the results along with corresponding damping ratio are presented in Table **??**. From the eigenvalue analysis it can be seen that there exists a zero eigen, for which the system is marginally stable. It means the system becomes stable, but not at the equilibrium.

Table 8: Electro-mechanical Modes of Oscillation of Base System

Most Associated States	**Eig (Real)**	**Eig (Imag)**	**Pseudo-Freq**	**Frequency**	**Damping Ratio (%)**
ω_5, δ_5	-0.1001	9.1659	1.4588	1.4589	1.0919
ω_5, δ_5	-0.1001	-9.1659	1.4588	1.4589	1.0919
ω_4, δ_4	-0.1201	8.3312	1.3260	1.3261	1.4415
ω_4, δ_4	-0.1201	-8.3312	1.3260	1.3261	1.4415
δ_3, ω_3	-0.1867	8.1713	1.3005	1.3008	2.2846
δ_3, ω_3	-0.1867	-8.1713	1.3005	1.3008	2.2846
ω_2, δ_2	-0.0207	7.6077	1.2108	1.2108	0.2725
ω_2, δ_2	-0.0207	-7.6077	1.2108	1.2108	0.2725
δ_1	0	0	0	0	-
ω_1	-0.18397	0	0	0	100

This marginal stability effect can also be observed from the time domain analysis in Figure 14. The frequency response of the generators show that the system becomes

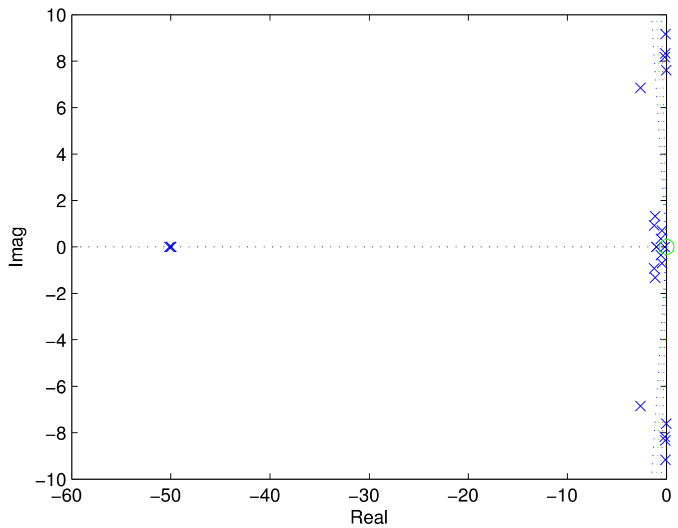

Figure 13: Eigenvalue plot of base case

stable not exactly at the equilibrium, but somewhere close to it.

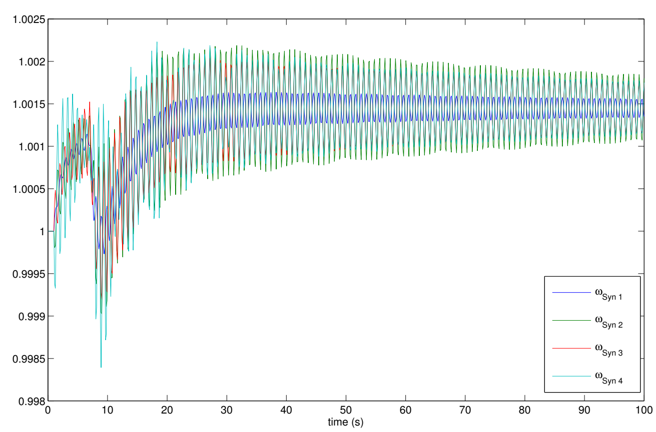

Figure 14: Frequency vs time response of synchronous generators

The results obtained in this study can be divided into 6 cases, as shown in Table 9. In each case, results are observed for different wind penetration levels. Starting from 1 p.u. or 27% penetration, it was decreased to as low as 0.93 p.u. (24%) and increased to as high as 1.5 p.u. (40%).

Table 9: Cases

Case No.	Case
1	Integrating DFIG
2	Integrating DDSG
3	Designing PSS for DFIG
4	Designing PSS for DDSG
5	Creating a Small Disturbance with DFIG Integrated
6	Creating a Small Disturbance with DDSG Integrated

4.2 Case 1: DFIG Integration

The synchronous generator at bus 3 is replaced by a DFIG. The real power penetration from this bus is kept at 1 p.u. or 27%, therefore the power flow results remain the same as in the base case shown in Table 7. However, the eigenvalue report in Table 10 show significant difference in result.

Table 10: Electro-mechanical modes of oscillation after DFIG Integration at 1 p.u.

Most Associated States	Eig (Real)	Eig (Imag)	Pseudo-Freq	Frequency	Damping Ratio (%)
ω_4, δ_4	-0.0971	9.1427	1.4551	1.4552	1.0619
ω_4, δ_4	-0.0971	-9.1427	1.4551	1.4552	1.0619
ω_3, δ_3	-0.1141	8.2651	1.3154	1.3156	1.3809
ω_3, δ_3	-0.1141	-8.2651	1.3154	1.3156	1.3809
ω_2, δ_2	-0.0642	7.9349	1.2629	1.2629	0.8096
ω_2, δ_2	-0.0642	-7.9349	1.2629	1.2629	0.8096
δ_1, ω_1	-0.0692	1.7024	0.2709	0.2712	4.0610
δ_1, ω_1	-0.0692	-1.7024	0.2709	0.2712	4.0610

It is seen from the eigenvalue analysis that there is no zero eigen. Therefore, after the DFIG integration, the system became asymptotically stable from marginally stable. Comparing with table **??**, it can be observed that even though the first two electromechanical modes participate less towards damping in case of DFIG, the difference is far too less than how much more generator 2 modes participate towards positive damping. Most importantly, generator 1 no longer participates towards a zero eigen, which ultimately stabilizes the system at the equilibrium. This can be explained from the physical origin of power system oscillations. In synchronous generators, the electrical torque is mainly dependent on the angle between rotor and stator flux. This angle is the integral of the difference in rotational speed between these two fluxes, eventually depending upon the difference between electrical and mechanical torque. This makes the mechanical part of the synchronous machine a second order system that shows oscillatory behavior by nature. Further, small changes in rotor speed hardly affects the electrical torque developed by the machine, as they hardly change the rotor angle. Therefore, the mechanical part of a synchronous system is naturally prone to weakly damped oscillations [3].

However, this does not apply to the generator types normally used in wind turbines. The variable speed wind turbines are decoupled from the grid by power electronic converters that control the rotor speed and electrical power, damping any rotor speed oscillations that may occur. Thus, variable speed wind turbines do not react to any oscillations that occur in the power system, because the generator does not notice them as they are not transferred through the converter. Therefore, they do not lead to power system oscillations either [3].

In this case, wind power replaces the power generated by synchronous generators. Therefore, the contribution of synchronous generators to the overall demand for power becomes less, even though the topology of the system stays unchanged. Thus, the synchronous generators become smaller relative to the impedances of the grid. This strengthens the mutual coupling, which in most cases improves the damping of any oscillations that occur between the synchronous generators [3]. Hence, as expected, the replacement of the synchronous generator by the wind turbine generator (in this case a DFIG) improved the overall damping of power system oscillations.

4.2.1 Decreasing Penetration

Table 11 shows the power flow results for decreased wind penetration from DFIG. If compared with Table 7, it can be seen that power generation from DFIG is lowered to 0.94 and 0.93 p.u. from 1 p.u. As a result, more power is drawn from generator 1 at the slack bus.

Table 11: Power flow report for decreased generation from DFIG

Unchanged with varied penetration				0.94 p.u.			0.93 p.u.		
Bus	**V**	**P load**	**Q load**	**phase**	**P gen**	**Q gen**	**phase**	**P gen**	**Q gen**
1	1.06	0.00	0.00	0.00	2.43	-0.14	0.00	2.44	-0.14
2	1.05	0.30	0.18	-0.09	0.40	0.41	-0.09	0.40	0.41
3	1.05	1.32	0.27	-0.19	0.94	0.55	-0.19	0.93	0.55
4	1.01	0.67	0.06	-0.19	0.00	0.00	0.19	0.00	0.00
5	1.01	0.11	0.02	-0.17	0.00	0.00	-0.17	0.00	0.00
6	1.07	0.16	0.11	-0.31	0.00	0.39	-0.31	0.00	0.39
7	1.04	0.00	0.00	-0.27	0.00	0.00	-0.27	0.00	0.00
8	1.09	0.00	0.00	-0.27	0.00	0.30	-0.27	0.00	0.30
9	1.02	0.41	0.23	-0.31	0.00	0.00	-0.31	0.00	0.00
10	1.02	0.13	0.08	-0.32	0.00	0.00	-0.32	0.00	0.00
11	1.04	0.05	0.03	-0.31	0.00	0.00	-0.31	0.00	0.00
12	1.05	0.09	0.02	-0.33	0.00	0.00	-0.33	0.00	0.00
13	1.04	0.19	0.08	-0.33	0.00	0.00	-0.33	0.00	0.00
14	1.00	0.21	0.07	-0.34	0.00	0.00	-0.34	0.00	0.00

Table 12 shows the eigenvalue report for lower penetration of DFIG. If compared with Table 10, apart from generator 3 electromechanical modes, the rest of the modes participate towards less damping. Hence, the overall damping of the system is decreased with decreased penetration.

Table 12: Electro-mechanical modes of oscillation for decreased penetration from DFIG

	0.94 p.u.			0.93		
Most Associated States	Real Eigenvalue	Imaginary Eigenvalue	Damping Ratio (%)	Real Eigenvalue	Imaginary Eigenvalue	Damping Ratio (%)
ω_4, δ_4	-0.0969	9.1451	1.0600	-0.0970	9.1447	1.0602
ω_4, δ_4	-0.0969	-9.1451	1.0600	-0.0970	-9.1447	1.0602
ω_3, δ_3	-0.1149	8.2700	1.3886	-0.1148	8.2693	1.3875
ω_3, δ_3	-0.1149	-8.2700	1.3886	-0.1148	-8.2693	1.3875
ω_2, δ_2	-0.0592	7.9474	0.7447	-0.0599	7.9456	0.7540
ω_2, δ_2	-0.0592	-7.9474	0.7447	-0.0599	-7.9456	0.7540
δ_1, ω_1	-0.0681	1.7066	3.9843	-0.0682	1.7058	3.9960
δ_1, ω_1	-0.0681	-1.7066	3.9843	-0.0682	-1.7058	3.9960

4.2.2 Increasing Penetration

Table 13 shows the power flow results for increased wind penetration from DFIG. If compared with Table 7, it can be seen that power generation from DFIG is increased to 1.23 and 1.5 p.u. from 1 p.u. As a result, less power is drawn from generator 1 at the slack bus.

Table 13: Power flow report for increased generation from DFIG

Unchanged with Varied Penetration				1.23 p.u.			1.5 p.u.		
Bus	**V**	**P load**	**Q load**	**phase**	**P gen**	**Q gen**	**phase**	**P gen**	**Q gen**
1	1.06	0.00	0.00	0.00	2.11	-0.08	0.00	1.83	-0.02
2	1.05	0.30	0.18	-0.08	0.40	0.35	-0.06	0.40	0.31
3	1.05	1.32	0.27	-0.14	1.23	0.45	-0.10	1.50	0.36
4	1.01	0.67	0.06	-0.17	0.00	0.00	-0.15	0.00	0.00
5	1.01	0.11	0.02	-0.15	0.00	0.00	-0.14	0.00	0.00
6	1.07	0.16	0.11	-0.29	0.00	0.39	-0.27	0.00	0.39
7	1.04	0.00	0.00	-0.25	0.00	0.00	-0.23	0.00	0.00
8	1.09	0.00	0.00	-0.25	0.00	0.30	-0.23	0.00	0.30
9	1.02	0.41	0.23	-0.29	0.00	0.00	-0.27	0.00	0.00
10	1.02	0.13	0.08	-0.30	0.00	0.00	-0.28	0.00	0.00
11	1.04	0.05	0.03	-0.29	0.00	0.00	-0.28	0.00	0.00
12	1.05	0.09	0.02	-0.31	0.00	0.00	-0.29	0.00	0.00
13	1.04	0.19	0.08	-0.31	0.00	0.00	-0.29	0.00	0.00
14	1.00	0.21	0.07	-0.32	0.00	0.00	-0.31	0.00	0.00

Table 14 presents the eigenvalue report for higher wind penetration from DFIG. Again, if compared with Table 10, apart from generator 3 electromechanical modes, the rest of the modes participates more towards positive damping. Hence the overall system damping is increased with increasing penetration.

Table 14: Electro-mechanical modes of oscillation for increased penetration of DFIG

	1.23 p.u.			1.5		
Most Associated States	Real Eigenvalue	Imaginary Eigenvalue	Damping Ratio (%)	Real Eigenvalue	Imaginary Eigenvalue	Damping Ratio (%)
ω_4, δ_4	-0.0976	9.1382	1.0675	-0.0981	9.1395	1.0730
ω_4, δ_4	-0.0976	-9.1382	1.0675	-0.0981	-9.1395	1.0730
ω_3, δ_3	-0.1122	8.2542	1.3595	-0.1108	8.2491	1.3425
ω_3, δ_3	-0.1122	-8.2542	1.3595	-0.1108	-8.2491	1.3425
ω_2, δ_2	-0.0801	7.9004	1.0141	-0.0972	7.8727	1.2348
ω_2, δ_2	-0.0801	-7.9004	1.0141	-0.0972	-7.8727	1.2348
δ_1, ω_1	-0.0727	1.7043	4.2600	-0.0766	1.7365	4.4074
δ_1, ω_1	-0.0727	-1.7043	4.2600	-0.0766	-1.7365	4.4074

4.3 Case 2: DDSG Integration

This time, the synchronous generator at bus 3 is replaced by a DDSG. The real power penetration from this bus is kept at 27%, therefore the power flow results remain same as in the base case shown in Table 7. However, the eigenvalue report in Table 15 show significant difference in results.

Table 15: Electro-mechanical modes of oscillation after DDSG integration at 1 p.u.

Most Associated States	Eig (Real)	Eig (Imag)	Pseudo-Freq	Frequency	Damping Ratio (%)
ω_4, δ_4	-0.0976	9.1425	1.4551	1.4552	1.0679
ω_4, δ_4	-0.0976	-9.1425	1.4551	1.4552	1.0679
ω_3, δ_3	-0.1148	8.2657	1.3155	1.3156	1.3884
ω_3, δ_3	-0.1148	-8.2657	1.3155	1.3156	1.3884
ω_2, δ_2	-0.0584	7.9325	1.2625	1.2625	0.7356
ω_2, δ_2	-0.0584	-7.9325	1.2625	1.2625	0.7356
δ_1, ω_1	-0.4567	1.0064	0.1602	0.1759	41.3253
δ_1, ω_1	-0.4567	-1.0064	0.1602	0.1759	41.3253

Similar to the DFIG integration of 1 p.u., it is seen from the eigenvalue analysis that there is no zero eigen for DDSG integration either. Therefore for similar reasons mentioned in case of DFIG, it can be said that after the DDSG integration the system becomes asymptotically stable from marginally stable.

4.3.1 Decreasing Penetration

When the wind penetration is decreased from 1 p.u. to 0.94 and 0.93 p.u., the power flow results remain the same as was observed in the case of DFIG as shown in Table 11.

Table 16 shows the eigenvalue report for lower penetration of DDSG. If compared with Table 15, all the electromechanical modes of oscillation participate towards less damping. Hence, the overall damping of the system is decreased with decreased penetration.

Table 16: Electro-mechanical modes of oscillation for decreased penetration of DDSG

	0.94 p.u.			0.93		
Most Associated States	Real Eigenvalue	Imaginary Eigenvalue	Damping Ratio (%)	Real Eigenvalue	Imaginary Eigenvalue	Damping Ratio (%)
ω_4, δ_4	-0.0962	9.1444	1.0517	-0.0962	9.1448	1.0514
ω_4, δ_4	-0.0962	-9.1444	1.0517	-0.0962	-9.1448	1.0514
ω_3, δ_3	-0.1143	8.2694	1.3821	-0.1144	8.2702	1.3832
ω_3, δ_3	-0.1143	-8.2694	1.3821	-0.1144	-8.2702	1.3832
ω_2, δ_2	-0.0467	7.9362	0.5881	-0.0458	7.9380	0.5770
ω_2, δ_2	-0.0467	-7.9362	0.5881	-0.0458	-7.9380	0.5770
δ_1, ω_1	-0.2005	1.3794	14.3815	-0.2001	1.3718	14.4332
δ_1, ω_1	-0.2005	-1.3794	14.3815	-0.2001	-1.3718	14.4332

The small signal stability analysis shows that with the lower penetration, the system is heading towards marginal stability like it was in the original case, as the damping ratio is significantly low.

4.3.2 Increasing Penetration

When the wind penetration is increased from 1 p.u. to 1.23 and 1.5 p.u., the power flow results are the same as it was observed in case of DFIG as shown in Table 13. Table 17 presents the eigenvalue report for higher wind penetration from DDSG. Again, if compared with Table 15, apart from generator 3 electromechanical modes, the rest of the modes participates more towards positive damping. Hence the overall system damping is increased with increasing penetration.

Table 17: Electro-mechanical modes of oscillation at increased penetration of DDSG

	1.23 p.u.			1.5		
Most Associated States	Real Eigenvalue	Imaginary Eigenvalue	Damping Ratio (%)	Real Eigenvalue	Imaginary Eigenvalue	Damping Ratio (%)
ω_4, δ_4	-0.0981	9.1385	1.0739	-0.0987	9.1403	1.0799
ω_4, δ_4	-0.0981	-9.1385	1.0739	-0.0987	-9.1403	1.0799
ω_3, δ_3	-0.1129	8.2552	1.3673	-0.1114	8.2507	1.3506
ω_3, δ_3	-0.1129	-8.2552	1.3673	-0.1114	-8.2507	1.3506
ω_2, δ_2	-0.0741	7.8993	0.9378	-0.0914	7.8723	1.1608
ω_2, δ_2	-0.0741	-7.8993	0.9378	-0.0914	-7.8723	1.1608
δ_1, ω_1	-0.5537	1.1827	42.4000	-0.6326	1.4135	40.8496
δ_1, ω_1	-0.5537	-1.1827	42.4000	-0.6326	-1.4135	40.8496

The small signal stability analysis shows that with the higher penetration, the system is more stable, as the damping ratio is significantly high.

4.4 Case 1 vs Case 2

A DFIG was integrated in case 1 and a DDSG was integrated in case 2. Wind penetration was varied and small signal stability analysis was done. The resultant eigenvalue plots between the two cases for each penetration level is compared in this section. Additionally, to observe whether the damping ratio obtained from the eigenvalue analysis holds true, time domain analysis was also done and the results are compared in this section.

Figure 15 compares the eigen plots and Figure 16 compares the frequency-time response between DFIG and DDSG integrated system at 1 p.u. wind penetration. It can be observed from the eigenvalue plots that for both DFIG and DDSG, there are 33 negative eigen, no zero or positive eigen and 8 complex pairs.

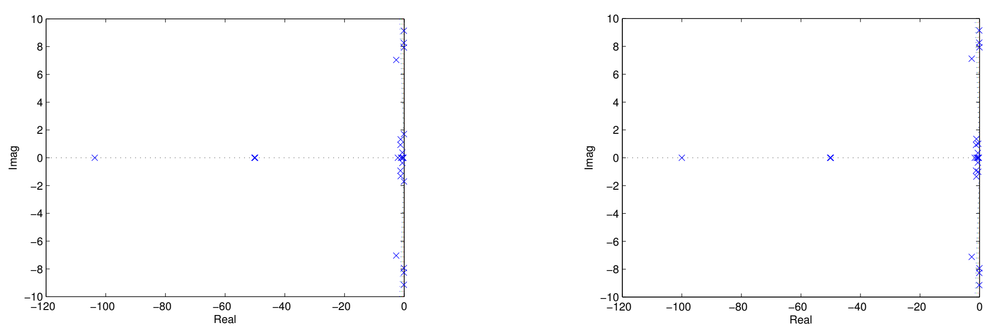

(a) DFIG at 1 p.u. (b) DDSG at 1 p.u.

Figure 15: Eigenvalue plots for 1 p.u. wind penetration

However, from the time domain analysis it is clear that the oscillation damps out faster in case of DDSG. This is reasonable as from the eigenvalues in Table 10 and Table 15 it can be seen that except for generator 2, all the modes provide more damping in case of DDSG. As a result, for the same penetration, the overall damping of the DDSG integrated system is slightly higher.

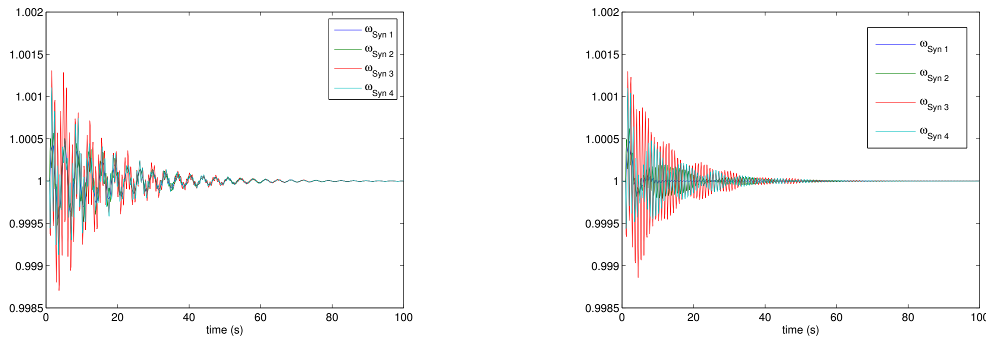

(a) DFIG at 1 p.u. (b) DDSG at 1 p.u.

Figure 16: Generator frequency vs time plots for 1 p.u. wind penetration

4.4.1 Lower Penetration

Figure 17 and Figure 18 compare the eigen plots between DFIG and DDSG integrated system at 0.94 p.u. and 0.93 p.u. wind penetration respectively. The eigenplots show that out of 33, all the eigenvalues have negative real parts and 8 of them are complex for both DFIG and DDSG.

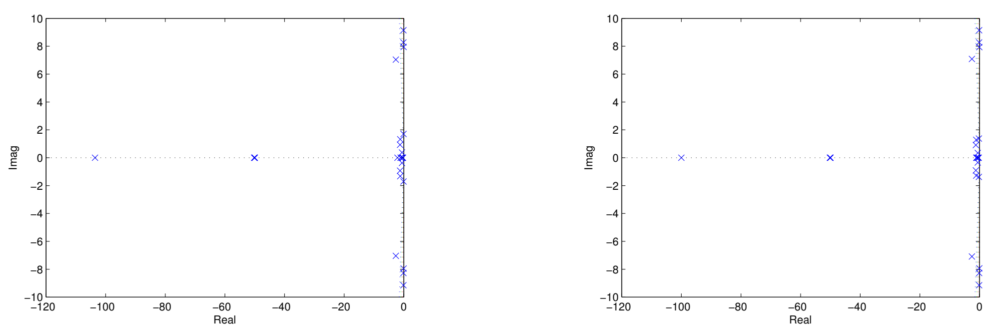

(a) DFIG at 0.94 p.u. (b) DDSG at 0.94 p.u.

Figure 17: Eigenvalue plots for 0.94 p.u. wind penetration

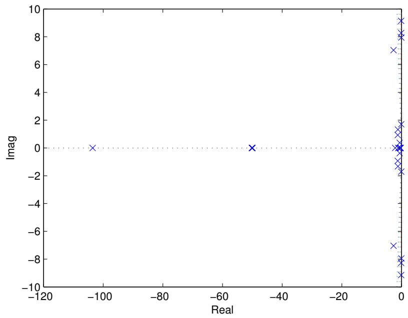

(a) DFIG at 0.93 p.u.

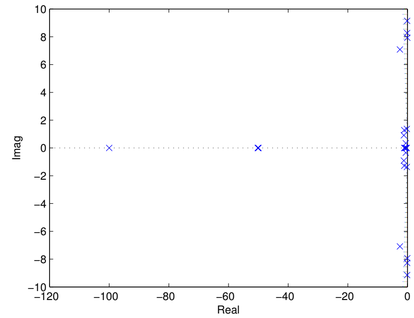

(b) DDSG at 0.93 p.u.

Figure 18: Eigenvalue plots for 0.93 p.u. wind penetration

Again, Figure 19 and Figure 20 compare the frequency-time response between DFIG and DDSG integrated system at 0.94 p.u. and 0.93 p.u. wind penetration respectively. The time domain simulation shows that even though DFIG integrated system exhibits more oscillation (Figure 19a), with lower penetration, the DDSG integrated system tries to move from the equilibrium (Figure 19b). Eventually it becomes marginally stable after around 16 seconds, for 0.93 p.u. wind penetration (Figure 20b). Whereas DFIG is not affected as much (Figure 20a).

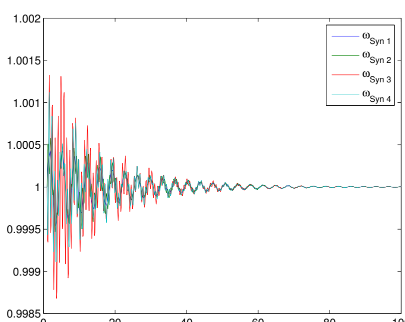

(a) DFIG at 0.94 p.u.

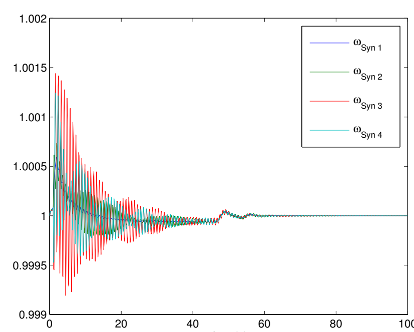

(b) DDSG at 0.94 p.u.

Figure 19: Generator frequency vs time plots for 0.94 p.u. wind penetration

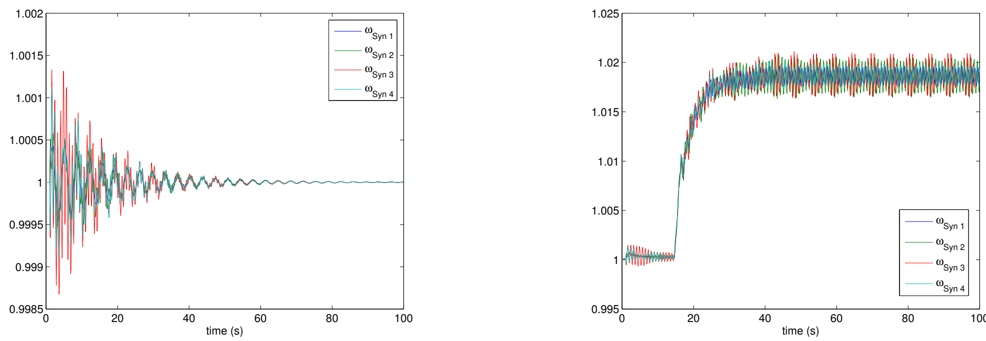

(a) DFIG at 0.93 p.u.

(b) DDSG at 0.93 p.u.

Figure 20: Generator frequency vs time plots for 0.93 p.u. wind penetration

4.4.2 Higher Penetration

Figure 21 and Figure 22 compare the eigen plots between DFIG and DDSG integrated system at 1.23 p.u. and 1.5 p.u. wind penetration respectively. If the eigenplots are closely observed, it is clear that compared to the lower penetration the eigens moved towards left for 1.23 and 1.5 p.u. penetration, meaning the real part became more negative. Nevertheless, out of 33, all the eigenvalues have negative real parts and 8 of them are complex.

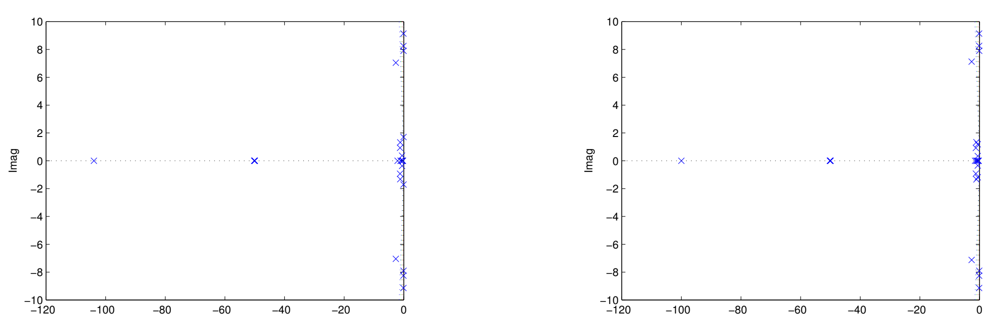

(a) DFIG at 1.23 p.u.

(b) DDSG at 1.23 p.u.

Figure 21: Eigenvalue plots for 1.23 p.u. wind penetration

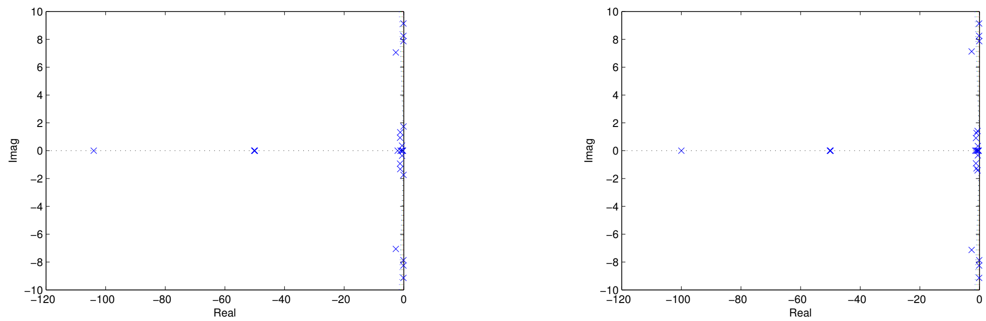

(a) DFIG at 1.5 p.u. (b) DDSG at 1.5 p.u.

Figure 22: Eigenvalue plots for 1.5 p.u. wind penetration

Again, Figure 23 and Figure 24 compare the frequency-time response between DFIG and DDSG integrated system at 1.23 p.u. and 1.5 p.u. wind penetration respectively. The time domain simulation shows that the DFIG integrated system exhibits more oscillation (Figure 23a), compared to the the DDSG integrated system (Figure 23b). Even though the oscillations are damped slightly faster (Figure 24a) at 1.5 p.u. than they did at 1.23 p.u., still better damping is clearly visible with DDSG (Figure 24b).

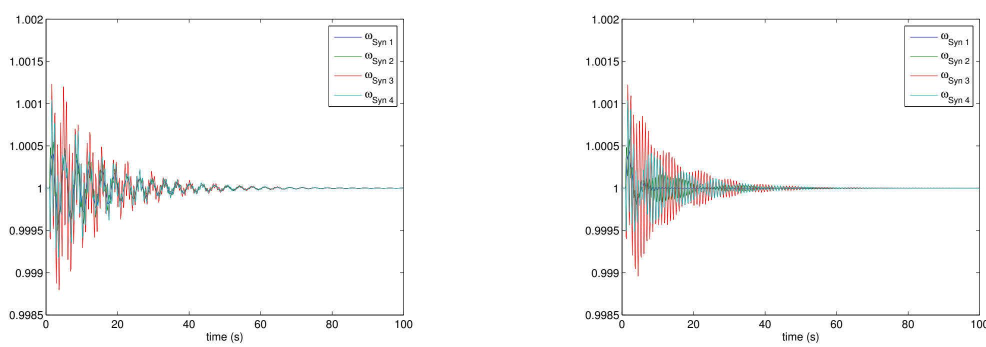

(a) DFIG at 1.23 p.u. (b) DDSG at 1.23 p.u.

Figure 23: Generator frequency vs time plots for 1.23 p.u. wind penetration

Therefore, it can be concluded that at a particular penetration level, DDSG integrated system damps out the oscillation faster by providing better damping, than the

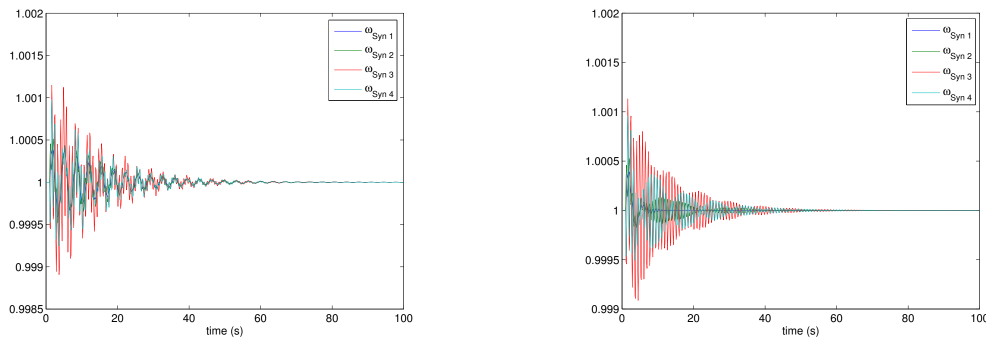

(a) DFIG at 1.5 p.u. (b) DDSG at 1.5 p.u.

Figure 24: Generator frequency vs time plots for 1.5 p.u. wind penetration

DFIG integrated systems. However, after a certain level of wind penetration, DDSG tends to move the system back to marginal stability, like it was originally. In this study, that level is found to be 0.93 p.u. DDSG fails to make the system asymptotically stable any longer when the penetration level reaches 0.93 p.u. or below. On the other hand, DFIG does not exhibit such drastic change in stability with the change of penetration.

This phenomenon can be explained from the characteristics equations of DFIG and DDSG presented in chapter 2. For DFIG, differential equations for the converter currents are as follows:

$$i_{qr,max} = -\,P_{min}$$

$$i_{qr,min} = -\,P_{max}$$

$$\dot{i_{qr}} = \left(-\frac{x_s + x_m}{x_m V} P^*_\omega(\omega_m)/\omega_m - i_{qr}\right)\frac{1}{T_e}$$

where $P^*_\omega(\omega_m)$ is the power-speed characteristic roughly optimizing the wind energy capture and is calculated using the current rotor speed value. x_s , x_m are the stator and magnetizing reactance of the generator, V is the grid voltage magnitude, ω_m is the rotor speed, and is T_e is the electrical torque.

For DDSG, following are the characteristic differential equations:

$$
\begin{aligned}
i_{qs,max} &= -P_{min} \\
i_{qs,min} &= -P_{max} \\
\dot{i_{qs}} &= (i_{qsref} - i_{qs})/T_\epsilon \\
i_{qsref} &= \frac{P^*_\omega(\omega_m)}{\omega_m(\psi_p - x_d i_{ds})}
\end{aligned}
$$

Where x_d is the stator d axis reactance and ψ_p is the rotor field flux.

Comparing the 2 sets of equation, it can be observed that the minimum and maximum real power delivered to the grid is related to rotor and stator q axis current for DFIG and DDSG respectively and the minimum power delivered is equal to maximum q axis current. Hence the q axis current is of primary interest here. For DDSG, the i_q is more sensitive to parameters x_d and ψ_p. Whereas for DFIG, i_q is not as sensitive to x_s or x_m , since x_m is usually much larger than x_s. As a result, for a smaller value of x_d, DDSG tends to perform well at higher penetration, and vice versa. In this thesis, the parameter x_d for DDSG was taken as low as 0.01 p.u., where as it can go up to 1.5 p.u. or higher, in which case it would perform well for lower penetration. On the other hand, DFIG is not as sensitive to the reactance value. Hence for a particular model, DFIG allows for a larger range of penetration, even though for a smaller range of penetration, DDSG might provide better stability.

4.5 Case 3: PSS Design for DFIG Integrated System

In order to improve the damping, PSSs are designed for the DFIG integrated system. From the electromechanical modes participating in the oscillation shown in Table 10, it is clear that generators 2, 3 and 4 oscillate with frequencies 7.93, 8.27 and 9.14 radians respectively. Hence the three PSSs design for these generators are quite similar. The following is the A matrix obtained from PSAT for 1 p.u. wind penetration:

$$\begin{bmatrix} a_{11} & a_{12} & a_{13} & a_{14} \\ a_{21} & a_{22} & a_{23} & a_{24} \\ a_{31} & a_{32} & a_{33} & a_{34} \\ a_{41} & a_{42} & a_{43} & a_{44} \end{bmatrix} = \begin{bmatrix} -0.19425 & -0.0306 & -0.06187 & 0 \\ 376.9911 & 0 & 0 & 0 \\ 0 & -0.01796 & -0.18691 & 0 \\ 0 & -27.2066 & 814.6482 & -1000 \end{bmatrix} \tag{84}$$

Generator 2 oscillates with a frequency of 7.93 radians. Hence the PSS design based on that and generator parameters:

From equation (57) to (76), using matlab,

$$\Delta T_e|_{\psi_{fd}} = 0.0033 - 0.0078i$$

$$K_{D(\Delta\psi fd)} = -\frac{0.0078 * 377}{7.93} = 0.37$$

From (79),(80),

$$\Delta T_{PSS} = 0.1497 - 0.3400i = 0.3715\angle - 66.24^{\circ} \tag{85}$$

Hence, the minimum gain from the PSS:

$$K_{PSS} = \frac{0.37}{0.0.34} = 1.1 \tag{86}$$

Again, since the angle that needs to be compensated is 45°, two phase compensation block compensating $\frac{66.24}{2} = 33°$ are needed. From (82):

$$T_1 = T_3 = 0.28s$$

$$T_1 = T_3 = 0.08s$$

Generator 3 oscillates with a frequency of 8.27 radians. Hence the PSS design based on that and generator parameters:

From equation (57) - (76), using matlab,

$$\Delta T_e|_{\psi_{fd}} = 0.0031 - 0.0066i$$

$$K_{D(\Delta\psi fd)} = -\frac{0.0066 * 377}{8.27} = 0.3$$

From (79),(80),

$$\Delta T_{PSS} = 0.1364 - 0.2800i = 0.31\angle - 64.03° \tag{87}$$

Hence, the minimum gain from the PSS:

$$K_{PSS} = \frac{0.3}{0.0.28} = 1.1 \tag{88}$$

Again, since the angle that needs to be compensated is 45°, two phase compensation block compensating $\frac{64.03}{2} = 32°$ are needed. From (82):

$$T_1 = T_3 = 0.27s$$

$$T_1 = T_3 = 0.08s$$

Generator 4 oscillates with a frequency of 9.14 radians. Hence the PSS design based on that and generator parameters:

Using same sets of equation in matlab,

$$\Delta T_e|_{\psi_{fd}} = 0.0025 - 0.0063i$$

$$K_{D(\Delta\psi fd)} = -\frac{0.0063 * 377}{9.14} = 0.26$$

$$\Delta T_{PSS} = 0.1113 - 0.2667i = 0.29\angle -67.35° \tag{89}$$

Hence, the minimum gain from the PSS:

$$K_{PSS} = \frac{0.26}{0.0.2667} = 0.97 \tag{90}$$

Again, since the angle that needs to be compensated is 45°, two phase compensation block compensating $\frac{67.35}{2} = 33.7°$ are needed. Therefore:

$$T_1 = T_3 = 0.29s$$

$$T_1 = T_3 = 0.08s$$

The eigenvalue analysis reports after designing the PSS, are shown in Table 18.

Comparing with the damping ratio in Table 10, it is visible that the damping of the system has been improved after adding the PSS.

Table 18: Electro-mechanical modes of oscillation with DFIG at 1 p.u. with PSS

Most Associated States	**Eig (Real)**	**Eig (Imag)**	**Pseudo-Freq**	**Frequency**	**Damping Ratio (%)**
ω_4, δ_4	-0.1577	9.2427	1.4710	1.4712	1.7062
ω_4, δ_4	-0.1577	-9.2427	1.4710	1.4712	1.7062
ω_3, δ_3	-0.1250	8.2286	1.3096	1.3098	1.5190
ω_3, δ_3	-0.1250	-8.2286	1.3096	1.3098	1.5190
ω_2, δ_2	-0.4071	8.4160	1.3394	1.3410	4.8311
ω_2, δ_2	-0.4071	-8.4160	1.3394	1.3410	4.8311
δ_1, ω_1	-0.2105	1.6761	0.2668	0.2689	12.4607
δ_1, ω_1	-0.2105	-1.6761	0.2668	0.2689	12.4607

4.5.1 Stability with PSS at Lower Penetration of DFIG

When the wind penetration is decreased from 1 p.u. to 0.94 and 0.93 p.u. respectively, the resulting eigenvalue analysis reports are shown in Table 19. Comparing with the values in Table 12, it can be observed that the damping of the system has been improved after the PSS design.

Table 19: Electro-mechanical modes of oscillation after PSS design for decreased penetration from DFIG

	0.94 p.u.			0.93		
Most Associated States	Real Eigenvalue	Imaginary Eigenvalue	Damping Ratio (%)	Real Eigenvalue	Imaginary Eigenvalue	Damping Ratio (%)
ω_4, δ_4	-0.1574	9.2445	1.7024	-0.1574	9.2448	1.7018
ω_4, δ_4	-0.1574	-9.2445	1.7024	-0.1574	-9.2448	1.7018
ω_3, δ_3	-0.1196	8.2277	1.4529	-0.1186	8.2276	1.4416
ω_3, δ_3	-0.1196	-8.2277	1.4529	-0.1186	-8.2276	1.4416
ω_2, δ_2	-0.4024	8.4283	4.7694	-0.4017	8.4304	4.7593
ω_2, δ_2	-0.4024	-8.4283	4.7694	-0.4017	-8.4304	4.7593
δ_1, ω_1	-0.2103	1.6799	12.4206	-0.2102	1.6807	12.4126
δ_1, ω_1	-0.2103	-1.6799	12.4206	-0.2102	-1.6807	12.4126

4.5.2 Stability with PSS at Higher Penetration of DFIG

With the designed PSS, when the wind penetration is increased from 1 p.u. to 1.23 and 1.5 p.u.respectively, the resulting eigenvalue analysis reports are shown in Table 20.

Comparing with the values in Table 14, it can be observed that the damping of the system has been improved after the PSS design.

Table 20: Electro-mechanical modes of oscillation at increased penetration from DFIG with PSS

	1.23 p.u.			1.5		
Most Associated States	Real Eigenvalue	Imaginary Eigenvalue	Damping Ratio (%)	Real Eigenvalue	Imaginary Eigenvalue	Damping Ratio (%)
ω_4, δ_4	-0.1591	9.2394	1.7216	-0.1609	9.2422	1.7407
ω_4, δ_4	-0.1591	-9.2394	1.7216	-0.1609	-9.2422	1.7407
ω_3, δ_3	-0.1438	8.2359	1.7458	-0.1604	8.2506	1.9440
ω_3, δ_3	-0.1438	-8.2359	1.7458	-0.1604	-8.2506	1.9440
ω_2, δ_2	-0.4255	8.3756	5.0739	-0.4494	8.3410	5.3795
ω_2, δ_2	-0.4255	-8.3756	5.0739	-0.4494	-8.3410	5.3795
δ_1, ω_1	-0.2114	1.6780	12.4963	-0.2127	1.7121	12.3305
δ_1, ω_1	-0.2114	-1.6780	12.4963	-0.2127	-1.7121	12.3305

4.6 Case 4: PSS Design for DDSG Integrated System

In order to improve the damping, PSSs are designed for the DDSG integrated system. From the electromechanical modes participating in the oscillation shown in Table 15, it is clear that generator 2, 3 and 4 oscillate with frequencies 7.93, 8.27 and 9.14 radians respectively. Hence the three PSSs design for these generators are quite similar. The following is the A matrix obtained from PSAT for 1 p.u. wind penetration:

$$\begin{bmatrix} a_{11} & a_{12} & a_{13} & a_{14} \\ a_{21} & a_{22} & a_{23} & a_{24} \\ a_{31} & a_{32} & a_{33} & a_{34} \\ a_{41} & a_{42} & a_{43} & a_{44} \end{bmatrix} = \begin{bmatrix} -0.19763 & -0.17784 & -0.01591 & 0 \\ 376.9911 & 0 & 0 & 0 \\ 0 & 0.020066 & -0.86508 & 0 \\ 0 & 17.03581 & 291.0661 & -1000 \end{bmatrix} \tag{91}$$

Generator 2 oscillates with a frequency of 7.93 radians. Hence the PSS is design based on that and generator parameters. From (57) - (76), using matlab,

$$\Delta T_e|_{\psi_{fd}} = -\,0.0003 + 0.0012i$$

$$K_{D(\Delta\psi fd)} = -\frac{0.0012 * 377}{7.93} = 0.057$$

From (79),(80),

$$\Delta T_{PSS} = 0.0244 - 0.0984i = 0.101\angle - 76.073^\circ \tag{92}$$

Hence, the minimum gain from the PSS:

$$K_{PSS} = \frac{0.057}{0.0984} = 0.6 \tag{93}$$

Again, since the angle that needs to be compensated is 45°, two phase compensation block compensating $\frac{76.073}{2} = 38^\circ$ are needed. From (82):

$$T_1 = T_3 = 0.3s$$

$$T_1 = T_3 = 0.07s$$

Generator 3 oscillates with a frequency of 8.27 radians. Hence the PSS design based on that and generator parameters:

Using same sets of equation in matlab,

$$\Delta T_e|_{\psi_{fd}} = -0.0002 + 0.00093i$$

$$K_{D(\Delta\psi fd)} = -\frac{0.00093 * 377}{8.27} = 0.04$$

$$\Delta T_{PSS} = 0.0179 - 0.0760i = 0.078\angle - 76.75^\circ \tag{94}$$

Hence, the minimum gain from the PSS:

$$K_{PSS} = \frac{0.04}{0.076} = 0.6 \tag{95}$$

Again, since the angle that needs to be compensated is 45°, two phase compensation block compensating $\frac{76.75}{2} = 38°$ are needed. Hence:

$$T_1 = T_3 = 0.3s$$

$$T_1 = T_3 = 0.07s$$

Generator 4 oscillates with a frequency of 9.14 radians. Hence the PSS design based on that and generator parameters:

Using same sets of equation in matlab,

$$\Delta T_e|_{\psi_{fd}} = -0.00017 + 0.00085i$$

$$K_{D(\Delta\psi fd)} = -\frac{0.00085 * 377}{9.14} = 0.035$$

From (79),(80),

$$\Delta T_{PSS} = 0.0149 - 0.0694i = 0.071\angle - 77.88° \tag{96}$$

Hence, the minimum gain from the PSS:

$$K_{PSS} = \frac{0.035}{0.0694} = 0.5 \tag{97}$$

Again, since the angle that needs to be compensated is 45°, two phase compensation block compensating $\frac{77.88}{2} = 39°$ are needed. Hence:

$$T_1 = T_3 = 0.3s$$

$$T_1 = T_3 = 0.065s$$

The eigenvalue analysis reports after the PSS design are shown in Table 21. Comparing with the values in Table 15, it is clear that the overall damping of the system has increased.

Table 21: Electro-mechanical modes of oscillation after PSS Design with DDSG at 1 p.u.

Most Associated States	**Eig (Real)**	**Eig (Imag)**	**Pseudo-Freq**	**Frequency**	**Damping Ratio (%)**
ω_4, δ_4	-0.3074	9.2447	1.4713	1.4722	3.3230
ω_4, δ_4	-0.3074	-9.2447	1.4713	1.4722	3.3230
ω_3, δ_3	-0.1334	8.1999	1.3051	1.3052	1.6269
ω_3, δ_3	-0.1334	-8.1999	1.3051	1.3052	1.6269
ω_2, δ_2	-0.4509	8.3488	1.3287	1.3307	5.3928
ω_2, δ_2	-0.4509	-8.3488	1.3287	1.3307	5.3928
δ_1, ω_1	-0.5476	0.8812	0.1402	0.1651	52.7835
δ_1, ω_1	-0.5476	-0.8812	0.1402	0.1651	52.7835

4.6.1 Stability with PSS at Lower Penetration of DDSG

With the PSS designed, when the wind penetration is decreased from 1 p.u. to 0.94 and 0.93 p.u. respectively, the eigenvalue analysis reports are shown in Table 22. Comparing with the values in Table 16, it can be observed that the damping of the system has been improved after the PSS design.

Table 22: Electro-mechanical modes of oscillation after PSS Design with DDSG at lower penetration

	0.94 p.u.			0.93		
Most Associated States	Real Eigenvalue	Imaginary Eigenvalue	Damping Ratio (%)	Real Eigenvalue	Imaginary Eigenvalue	Damping Ratio (%)
ω_4, δ_4	-0.3041	9.2502	3.2852	-0.3039	9.2506	3.2836
ω_4, δ_4	-0.3041	-9.2502	3.2852	-0.3039	-9.2506	3.2836
ω_3, δ_3	-0.1219	8.1952	1.4867	-0.1210	8.1950	1.4768
ω_3, δ_3	-0.1219	-8.1952	1.4867	-0.1210	-8.1950	1.4768
ω_2, δ_2	-0.4403	8.3603	5.2590	-0.4392	8.3628	5.2451
ω_2, δ_2	-0.4403	-8.3603	5.2590	-0.4392	-8.3628	5.2451
δ_1, ω_1	-0.3638	1.3240	26.4945	-0.3630	1.3156	26.5993
δ_1, ω_1	-0.3638	-1.3240	26.4945	-0.3630	-1.3156	26.5993

4.6.2 Stability with PSS at Higher Penetration of DDSG

When the wind penetration is increased from 1 p.u. to 1.23 and 1.5 p.u. respectively, the resulting eigenvalue analysis reports are shown in Table 23. Comparing with the values in Table 17, it can be observed that the damping of the system has been improved after the PSS design.

Table 23: Electro-mechanical modes of oscillation after PSS Design for increased penetration from DDSG.

	1.23 p.u.			1.5		
Most Associated States	Real Eigenvalue	Imaginary Eigenvalue	Damping Ratio (%)	Real Eigenvalue	Imaginary Eigenvalue	Damping Ratio (%)
ω_4, δ_4	-0.3119	9.2407	3.3734	-0.3175	9.2425	3.4328
ω_4, δ_4	-0.3119	-9.2407	3.3734	-0.3175	-9.2425	3.4328
ω_3, δ_3	-0.1458	8.2102	1.7757	-0.1549	8.2248	1.8825
ω_3, δ_3	-0.1458	-8.2102	1.7757	-0.1549	-8.2248	1.8825
ω_2, δ_2	-0.4757	8.3025	5.7199	-0.5071	8.2637	6.1251
ω_2, δ_2	-0.4757	-8.3025	5.7199	-0.5071	-8.2637	6.1251
δ_1, ω_1	-0.6548	0.9979	54.8595	-0.9401	1.5646	51.5019
δ_1, ω_1	-0.6548	-0.9979	54.8595	-0.9401	-1.5646	51.5019
δ_1, ω_1	-	-	-	-0.7966	1.0839	59.2217
δ_1, ω_1	-	-	-	-0.7966	-1.0839	59.2217

4.7 Comparison between Case 3 and Case 4

After the PSSs are designed, the results were different for DFIG and DDSG integrated systems. From the damping ratios obtained, it is clear that the overall damping of the system is improved for each penetration level when the PSSs are added. In this section, comparison is made between DFIG and DDSG integrated system damping after the PSSs are added.

Figure 25 compares the eigenvalue plots obtained from DFIG and DDSG integrated system for a wind penetration of 1 p.u. after the PSS is added. If compared with the plots in Figure 15, it is clear that for both DFIG and DDSG eigens moved towards negative, increasing the damping of the system. Also, comparing between Figure 25a and Figure 25b it is visible that DDSG has 11 pairs of complex eigenvalues, whereas DFIG has 9 which explains the results found in the time domain simulations later.

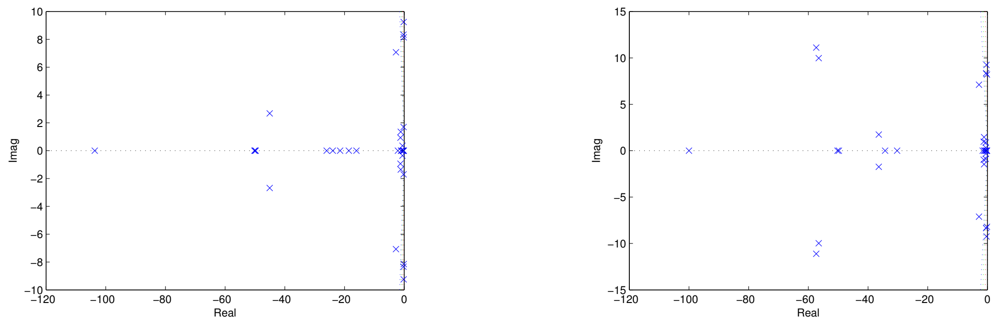

(a) DFIG at 1 p.u.

(b) DDSG at 1 p.u.

Figure 25: Eigenvalue plots for 1 p.u. wind penetration

For the same penetration, Figure 26 compares the time domain simulation, i.e. the frequency-time response of the system between DFIG and DDSG integrated systems. It can be observed from the plots that with the designed PSS, both DFIG and DDSG integrated systems damp out the oscillations faster. With PSS, both WTGs tend to damp them out at around 40 seconds, with DFIG 4-5 seconds sooner than DDSG.

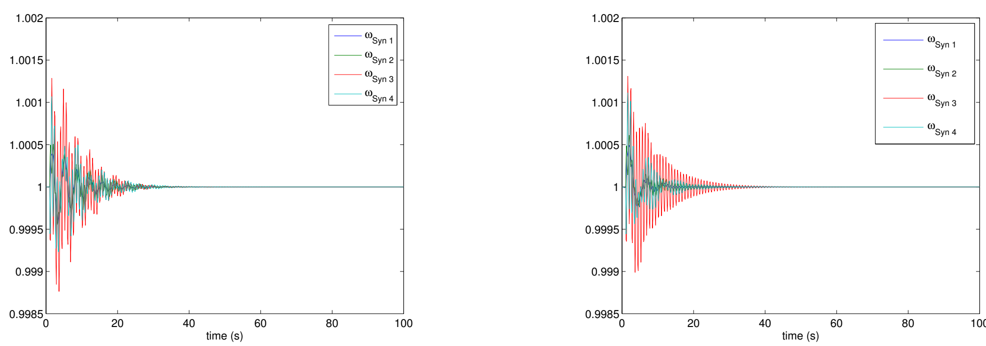

(a) DFIG at 1 p.u.

(b) DDSG at 1 p.u.

Figure 26: Generator frequency vs time plot for 1 p.u. wind penetration

4.7.1 Lower Penetration

Figure 27 and Figure 28 compare the eigenvalue plots obtained from DFIG and DDSG integrated system for 0.94 and 0.93 p.u. wind penetration respectively after the PSS is added. Comparing with the plots in Figure 17 and Figure 18, the eigens moved towards left, increasing the overall damping. Also, after adding the PSS, the DDSG integrated system exhibits 11 pairs of complex eigenvalues, whereas DFIG integrated system exhibits 9.

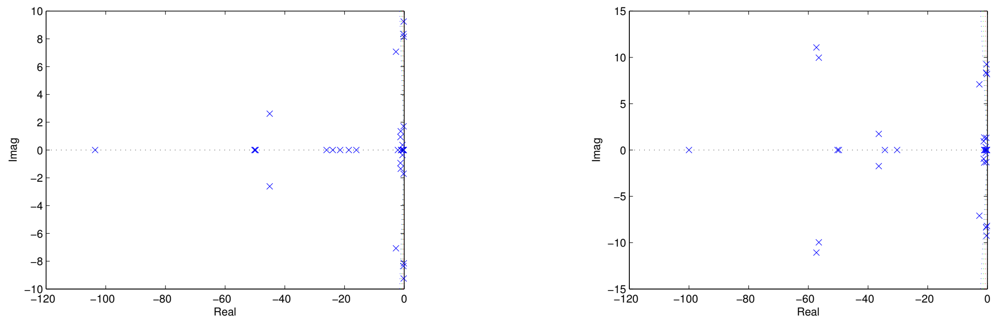

(a) DFIG at 0.94 p.u.

(b) DDSG at 0.94 p.u.

Figure 27: Eigenvalue plots for decreased wind penetration

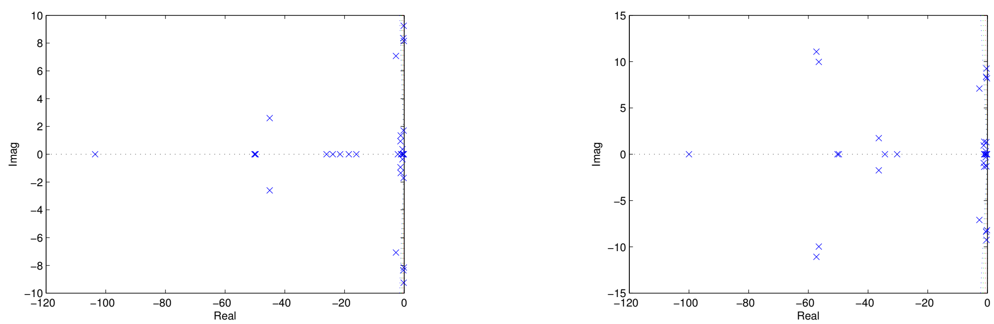

(a) DFIG at 0.93 p.u.

(b) DDSG at 0.93 p.u.

Figure 28: Eigenvalue plots for decreased wind penetration

The time domain simulation, i.e. the frequency-time response of the system between DFIG and DDSG integrated systems for 0.94 and 0.93 p.u. wind integration after adding the PSSs are compared in Figure 29 and Figure 30 respectively. For DFIG, the oscillation damps out within 40 seconds, which is much faster than without PSS presented in Figure 19a and Figure 20a. On the other hand, for DDSG, the system tended to move away from equilibrium (Figure 19b) previously without PSS. After adding the PSS, the system remains in the equilibrium state (Figure 29b). However, in case of 0.93 p.u. penetration from DDSG, the PSS was able to keep the system at equilibrium point till 30 seconds, unlike the case without any PSS where it took off from equilibrium state at as early as 18 seconds (Figure 20b).

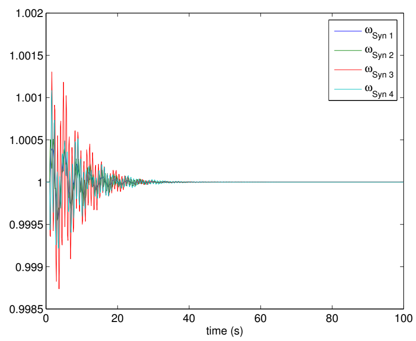

(a) DFIG at 0.94 p.u.

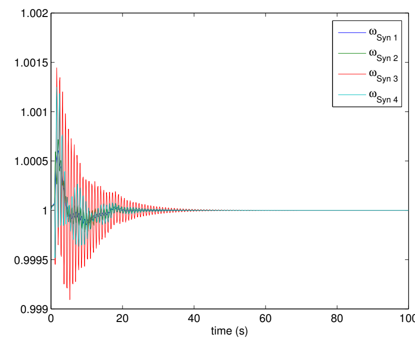

(b) DDSG at 0.94 p.u.

Figure 29: Generator frequency vs time plots for decreased wind penetration

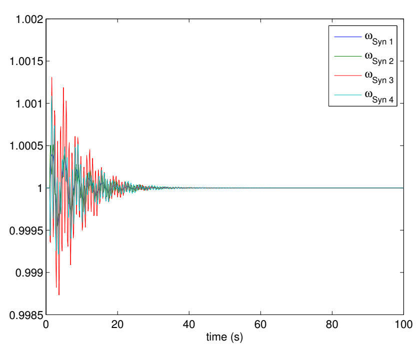

(a) DFIG at 0.93 p.u.

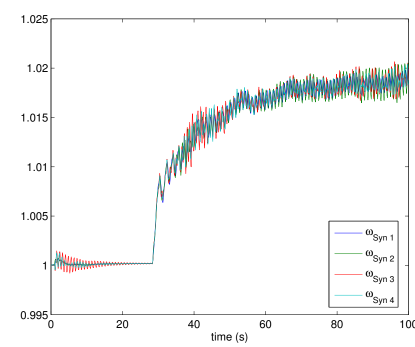

(b) DDSG at 0.93 p.u.

Figure 30: Generator frequency vs time plots for decreased wind penetration

4.7.2 Higher Penetration

Figure 31 and Figure 32 compare the eigenvalue plots obtained from DFIG and DDSG integrated system for 1.23 and 1.5 p.u. wind penetration respectively after the PSS is added. Comparing with the plots in Figure 21 and Figure 22 where no PSS was added, the eigens moved towards left, increasing the overall damping. Also, after adding the PSS, the DDSG integrated system exhibits 11 pairs of complex eigenvalues, whereas DFIG integrated system exhibits 9.

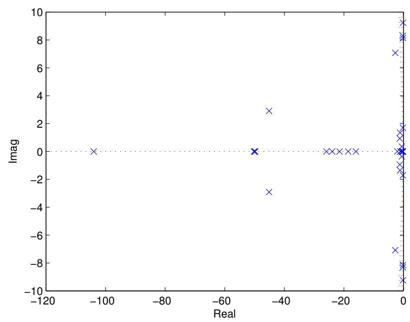

(a) DFIG at 1.23 p.u.

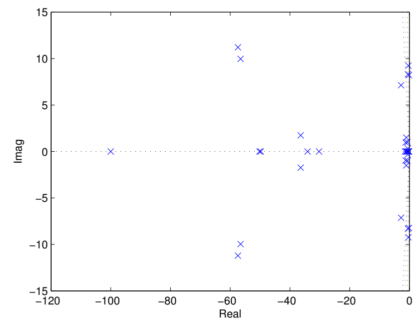

(b) DDSG at 1.23 p.u.

Figure 31: Eigenvalue plots for increased wind penetration

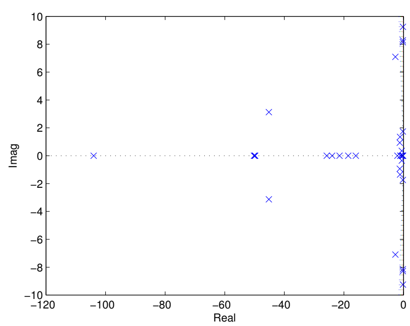

(a) DFIG at 1.5 p.u.

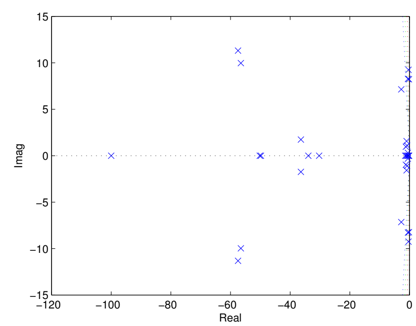

(b) DDSG at 1.5 p.u.

Figure 32: Eigenvalue plots for increased wind penetration

The time domain simulation, i.e. the frequency-time response of the system between DFIG and DDSG integrated systems for 1.23 and 1.5 p.u. wind integration after adding the PSS are compared in Figure 33 and Figure 34 respectively. For DFIG, the oscillation damps out within 40 seconds, which is much faster than without PSS presented in Figure 23a (100 seconds) and Figure 20a (80 seconds). On the other hand, for DDSG, the oscillations damp out within 38 seconds (Figure 23b and 24b), which is much faster than without PSS presented in Figure 23b and Figure 24b where it takes almost 60 seconds to damp out all the oscillations.

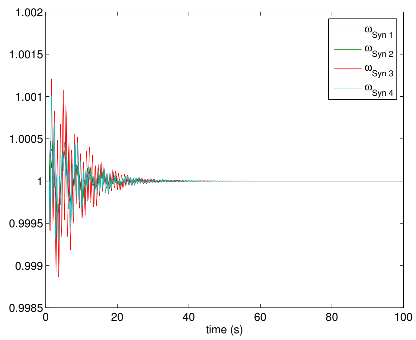

(a) DFIG at 1.23 p.u.

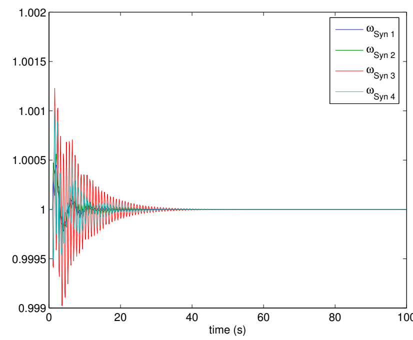

(b) DDSG at 1.23 p.u.

Figure 33: Generator frequency vs time plots for 1.23 p.u. wind penetration

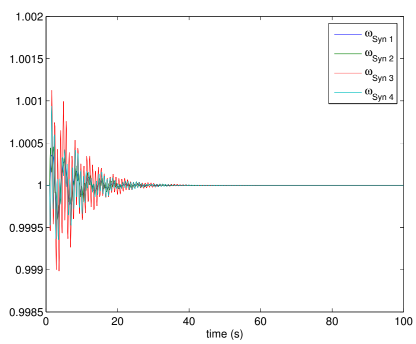

(a) DFIG at 1.5 p.u.

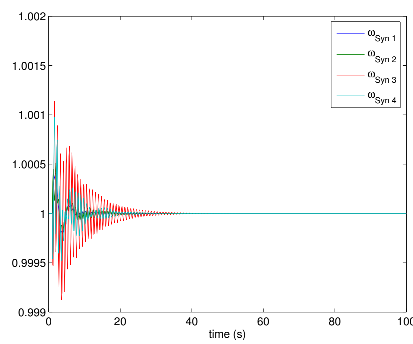

(b) DDSG at 1.5 p.u.

Figure 34: Generator frequency vs time plots for 1.5 p.u. wind penetration

Hence, with the designed PSSs added, the oscillations in the DDSG or DFIG integrated systems are damped out 22-60 seconds faster.

4.8 Case 5: Small Disturbance in DFIG Integrated System

A three phase fault occurs at bus 12 at 7th second and clears at 7.25th second. This causes the system to lose 2.3% load of the system for 0.25 seconds. For this case, a time domain analysis of the DFIG integrated system is done without and with the PSSs designed.

For 1 p.u. wind penetration, Figure 35a and Figure 35b show the time domain analysis of the system without and with the PSS respectively. The frequency response of the generators shows that with the PSSs, the oscillations damp out within 50 seconds of the fault clearance whereas without any PSS added, it takes at least 100 seconds.

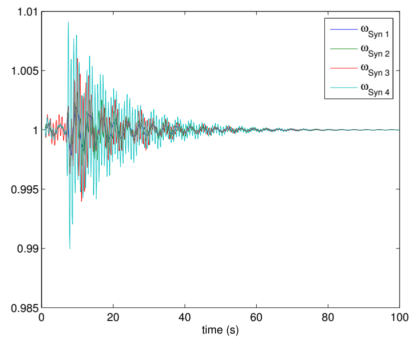

(a) Before adding PSS

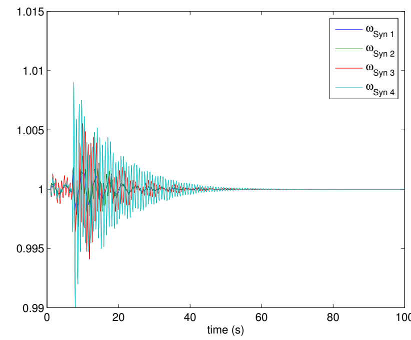

(b) With the designed PSS

Figure 35: Generator frequency vs time plot with small disturbance before and after adding PSS in 1 p.u. DFIG integrated system

4.8.1 Stability with Disturbance at Lower Penetration without and with the PSS

When the wind penetration is decreased to 0.94 p.u. from 1 p.u., Figure 36a and Figure 36b show the time domain analysis of the system without and with the PSS respectively. It can be observed from the frequency response of the generators that even at lower penetration the oscillations are damped out within 50 seconds of the fault clearance when the PSSs are added. Without the PSSs, it takes around 100 seconds to damp them out.

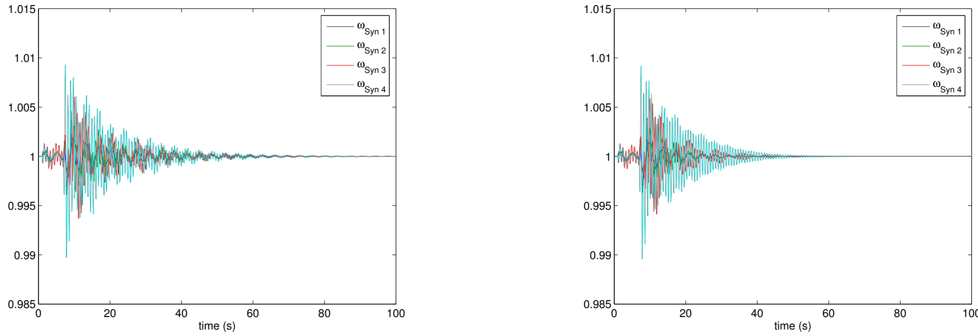

(a) Before adding PSS (b) With the designed PSS

Figure 36: Generator frequency vs time plot with small disturbance before and after adding PSS in 0.94 p.u. DFIG integrated system

For 0.93 p.u. wind penetration, Figure 37a and Figure 37b show the time domain analysis of the system without and with the PSS respectively. The results are similar to what they were for 0.94 p.u. penetration. The oscillations damp out at around 100 seconds without, and within 50 seconds of the fault clearance with the PSSs added.

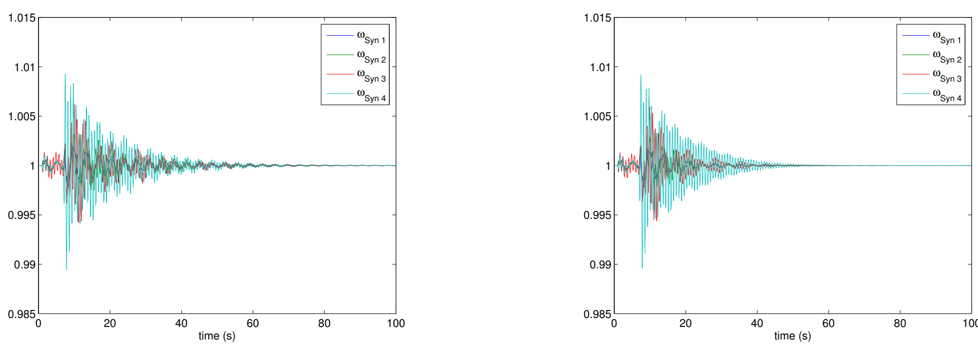

(a) Before adding PSS (b) With the designed PSS

Figure 37: Generator frequency vs time plot with small disturbance before and after adding PSS in 0.93 p.u. DFIG integrated system

4.8.2 Stability with Disturbance at Higher Penetration without and with the PSS

When the wind penetration is increased to 1.23 p.u. from 1 p.u., Figure 38a and Figure 38b show the time domain analysis of the system without and with the PSS respectively. The frequency response curves show that the oscillations are damped out within 45 seconds of the fault clearance when the PSS are added. Where as without the PSSs, it takes around 100 seconds.

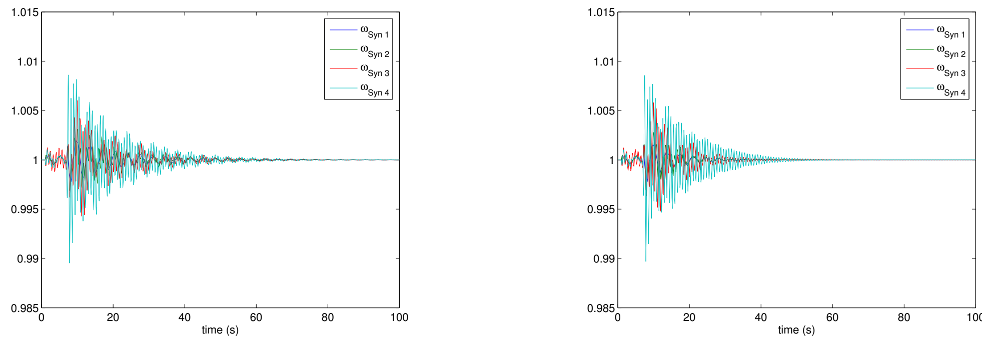

(a) Before adding PSS (b) With the designed PSS

Figure 38: Generator frequency vs time plot with small disturbance before and after adding PSS in 1.23 p.u. DFIG integrated system

For 1.5 p.u. wind penetration, Figure 39a and Figure 39b show the time domain analysis of the system without and with the PSS respectively. The results are similar to those at 1.23 p.u. penetration, where the oscillations damp out within 45 seconds of the fault clearance when the PSS added. Without the PSS however, it takes at least 100 seconds for the oscillations to damp out.

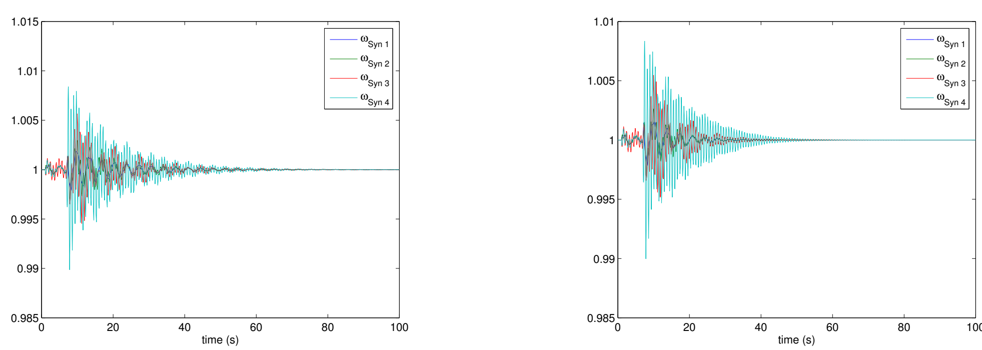

(a) Before adding PSS (b) With the designed PSS

Figure 39: Generator frequency vs time plot with small disturbance before and after adding PSS in 1.5 p.u. DFIG integrated system

4.9 Case 6: Small Disturbance in DDSG Integrated System

A three phase fault occurs in bus 12 at 7th seconds and clears at 7.25th second. This causes the system to lose 2.3% load of the system for 0.25 seconds. For this case, a time domain analysis is done for the DDSG integrated system without and with the PSSs designed.

For 1 p.u. wind penetration, Figure 40a and Figure 40b show the time domain analysis of the system without and with the PSS respectively. It can be observed from the frequency response of the generators that without the PSSs, the oscillations take around 80 seconds to damp out where as after adding the PSS they damp out within 40 seconds of the fault clearance.

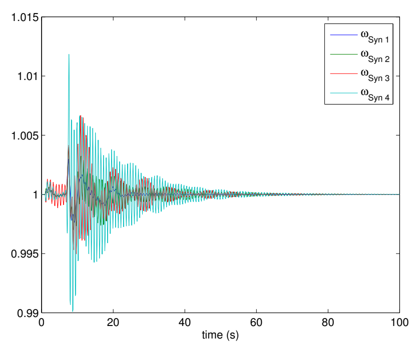

(a) Before adding PSS

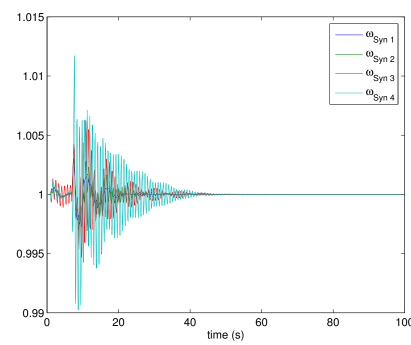

(b) With the designed PSS

Figure 40: Generator frequency vs time plot with small disturbance before and after adding PSS in 1 p.u. DDSG integrated system

4.9.1 Stability with Disturbance at Lower Penetration without & with the PSS

When the wind penetration is decreased to 0.94 p.u. from 1 p.u., Figure 41a and Figure 41b show the time domain analysis of the system without and with the PSS respectively. It can be observed from the frequency response of the generators that without the PSSs, the system tends to move away from the equilibrium at around 70th second, but it gets back right after. The oscillations however damp out within around 80 seconds of the fault clearance. On the other hand, with the PSSs, the system has no tendency to move away from the equilibrium, and the oscillations damp out within 50 seconds of the fault clearance.

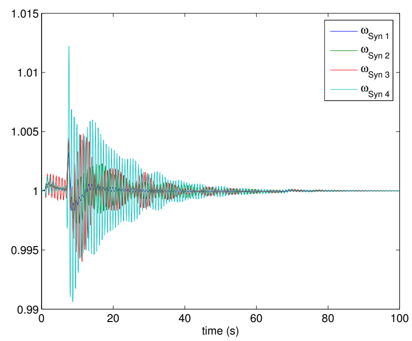

(a) Before adding PSS

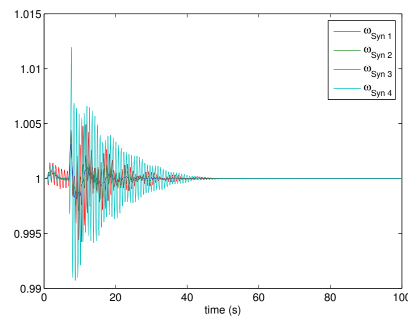

(b) With the designed PSS

Figure 41: Generator frequency vs time plot with small disturbance before and after adding PSS in 0.94 p.u. DDSG integrated system

For 0.93 p.u. wind penetration, Figure 42a and Figure 42b show the time domain analysis of the system without and with the PSS respectively. It can be observed from the frequency response of the system that without the PSSs, the system moves away from the equilibrium within 20 seconds of the fault before the oscillations are damped out and heads towards marginally stability. Whereas with the PSS, the oscillations are damped out within 45 seconds of the fault clearance, even though eventually at around 70th second, the system leaves the equilibrium state and heads towards marginal stability.

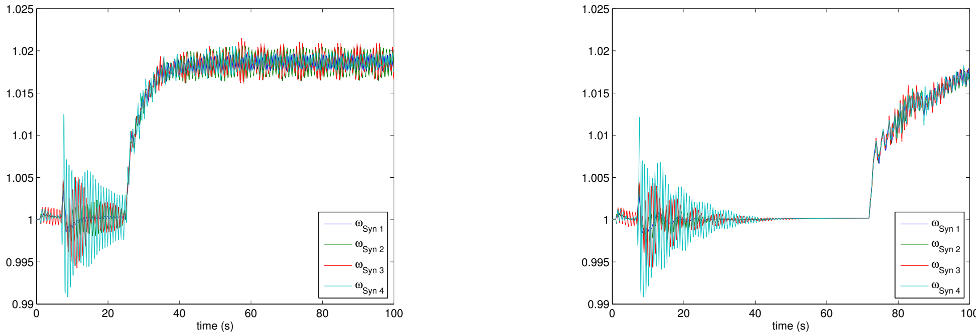

(a) Before adding PSS

(b) With the designed PSS

Figure 42: Generator frequency vs time plot with small disturbance before and after adding PSS in 0.93 p.u. DDSG integrated system

4.9.2 Stability with Disturbance at Higher Penetration without and with the PSS

When the wind penetration is increased to 1.23 p.u. from 1 p.u., Figure 43a and Figure 43b show the time domain analysis of the system without and with the PSS respectively. The frequency response of the generators show that the oscillations are damped out within 65 seconds of the fault clearance without any PSS in the system. When the PSSs are added, the oscillations damp out within 45 seconds of the fault clearance.

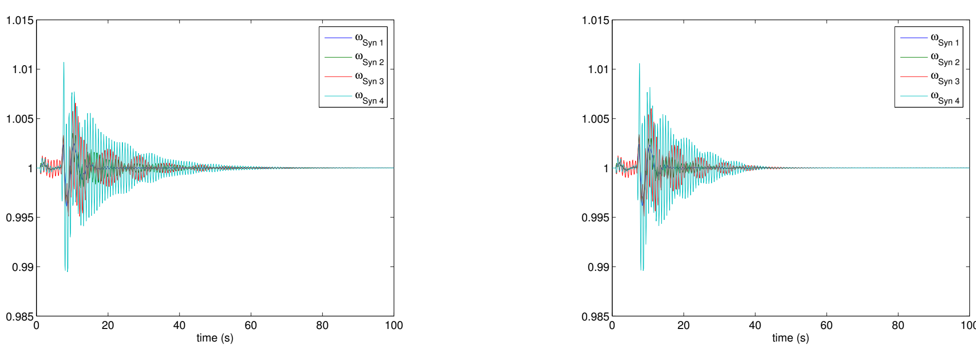

(a) Before adding PSS

(b) With the designed PSS

Figure 43: Generator frequency vs time plot with small disturbance before and after adding PSS in 1.23 p.u. DDSG integrated system

For 1.5 p.u. wind penetration, Figure 44a and Figure 44b show the time domain analysis of the system without and with the PSS respectively. The frequency response of the generators show that the oscillations are damped out within 60 seconds of the fault clearance without any PSS in the system. When the PSSs are added, the oscillations damp out within 40 seconds of the fault clearance.

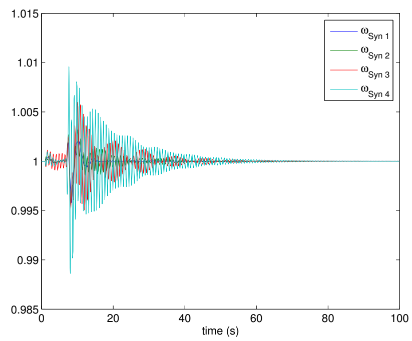

(a) Before adding PSS

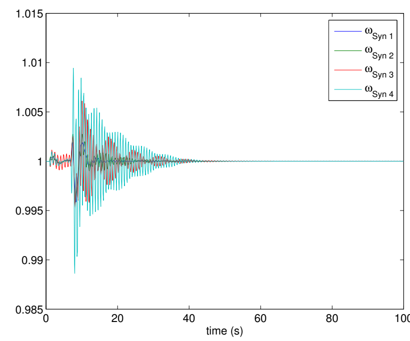

(b) With the designed PSS

Figure 44: Generator frequency vs time plot with small disturbance before and after adding PSS in 1.5 p.u. DDSG integrated system

4.10 DFIG vs DDSG Summary

Table 24 compares the damping ratio between DFIG and DDSG for 0.93, 0.94, 1, 1.23 and 1.5 p.u. wind penetration before adding the PSS. It can be observed that for DDSG, the damping ratio corresponding to all the electromechanical modes of oscillation decreases when the wind penetration is below 1 p.u. Specially the damping ratio corresponding to δ_1, ω_1 significantly drops. Where as for DFIG, the decrease is much less for all the modes. In fact, δ_3, ω_3 participate towards positive damping with lower penetration. Hence, the overall impact of lower wind penetration is more on DDSG integrated system than it is on DFIG integrated system. Which means even though with the decrease in wind penetration the overall system damping decreases for both DFIG and DDSG, DDSG integrated system exhibits a greater drop in damping ratio. As a result, at 0.93 p.u. wind penetration, DFIG integrated system exhibits higher overall damping than DDSG integrated system.

Table 24: Comparison between damping ratio of DFIG and DDSG integrated system without PSS at different wind penetration

	0.93		0.94		1		1.23		1.5	
States	**DFIG**	**DDSG**	**DFIG**	**DDSG**	**DFIG**	**DDSG**	**DFIG**	**DDSG**	**DFIG**	**DDSG**
ω_4, δ_4	1.0600	1.0514	1.0602	1.0517	1.0619	1.0679	1.0675	1.0739	1.0730	1.0799
ω_4, δ_4	1.0600	1.0514	1.0602	1.0517	1.0619	1.0679	1.0675	1.0739	1.0730	1.0799
δ_3, ω_3	1.3886	1.3832	1.3875	1.3821	1.3809	1.3884	1.3595	1.3673	1.3425	1.3506
δ_3, ω_3	1.3886	1.3832	1.3875	1.3821	1.3809	1.3884	1.3595	1.3673	1.3425	1.3506
ω_2, δ_2	0.7447	0.5770	0.7540	0.5881	0.8096	0.7356	1.0141	0.9378	1.2348	1.1608
ω_2, δ_2	0.7447	0.5770	0.7540	0.5881	0.8096	0.7356	1.0141	0.9378	1.2348	1.1608
δ_1, ω_1	3.9843	14.4332	3.9960	14.3815	4.0610	41.3253	4.2600	42.4000	4.4074	40.8496
δ_1, ω_1	3.9843	14.4332	3.9960	14.3815	4.0610	41.3253	4.2600	42.4000	4.4074	40.8496

On the other hand, with higher penetration, the overall damping of the system improves both for DFIG and DDSG integrated systems. Specially damping ratios corresponding to δ_1, ω_1 are significantly high for DDSG integrated system. Also, the increase in damping ratio corresponding to δ, ω of generator 2 and 4 is also higher in case of DDSG integrated system than it is in case of DFIG integrated system. As a result, at 1.5 p.u. wind penetration, DDSG integrated system exhibits higher overall damping than DFIG integrated system.

Table 25 compares the damping ratio between DFIG and DDSG for 0.93, 0.94, 1, 1.23 and 1.5 p.u. wind penetration after adding the PSS. Comparing with Table 24, it can be observed that all the damping ratios improved with PSS. Also, the decrease and increase of damping ratio with the decrease and increase of wind penetration remain consistent for both DFIG and DDSG integrated systems. The damping decreases when the wind penetration is low and the damping increases when the penetration is high.

Table 25: Comparison between damping ratio of DFIG and DDSG integrated system with PSS at different wind penetration

	0.93		0.94		1		1.23		1.5	
States	**DFIG**	**DDSG**	**DFIG**	**DDSG**	**DFIG**	**DDSG**	**DFIG**	**DDSG**	**DFIG**	**DDSG**
ω_4, δ_4	1.7018	3.2836	1.7024	3.2852	1.7062	3.3230	1.7216	3.3734	1.7407	3.4328
ω_4, δ_4	1.7018	3.2836	1.7024	3.2852	1.7062	3.3230	1.7216	3.3734	1.7407	3.4328
δ_3, ω_3	1.4416	1.4768	1.4529	1.4867	1.5190	1.6269	1.7458	1.7757	1.9440	1.8825
δ_3, ω_3	1.4416	1.4768	1.4529	1.4867	1.5190	1.6269	1.7458	1.7757	1.9440	1.8825
ω_2, δ_2	4.7593	5.2451	4.7694	5.2590	4.8311	5.3928	5.0739	5.7199	5.3795	6.1251
ω_2, δ_2	4.7593	5.24510	4.7694	5.2590	4.8311	5.3928	5.0739	5.7199	5.3795	6.1251
δ_1, ω_1	12.4126	26.5993	12.4206	26.4945	12.4607	52.7835	12.4963	54.8595	12.3305	51.5019
δ_1, ω_1	12.4126	26.5993	12.4206	26.4945	12.4607	52.7835	12.4963	54.8595	12.3305	51.5019

It can be observed from Table 25 that for each level of penetration, DDSG integrated system exhibits more damping than the DFIG integrated system. On the other hand, after adding the PSSs, the DDSG integrated system has 11 complex pairs of eigenvalues and DFIG has only 9. As a result, time domain simulations presented in section 1.7 shows that the oscillations in DFIG and DDSG integrated systems damp out at around the same time for wind penetration 0.94 p.u. or higher. Although at 0.93 p.u., DDSG system seems to have higher damping ratio than DFIG, it is seen from the frequency response of the generators that unlike DFIG, the DDSG integrated system becomes marginally stable after a certain time (Figure 30b). This is due to the dependency of DDSG converter q axis current on the stator q axis reactance, as discussed in section 1.4.

Also, at 1.5 p.u. (40% penetration), the highest wind penetration considered in this study, the damping ratio corresponding to δ_1, ω_1 drops for both DDSG and DFIG integrated systems. Similar was the case with DDSG without PSS (Table 24) This phenomenon can be explained by the weak grid. No commercially available wind or utility-scale solar PV generation is capable of operation in a system without the stabilizing benefit of synchronous machines. There is a point at which the amount of short-circuit strength provided by synchronous machines becomes insufficient and operation becomes impossible. "Weak grid" is a generic term that describes operating near that point [26]. Hence with the wind penetration increasing above 40%, the decrease in damping ratio might mean the system is moving towards weak grid condition.

CHAPTER 5: CONCLUSION AND FUTURE WORK

5.1 Conclusion

The objective of the thesis was to integrate two types of variable speed wind turbine generators, DFIG and DDSG one at a time and observe their impact on the small signal stability of the system. Research related to the stability of DFIG integrated systems has been going on for quite sometime, whereas DDSG is comparatively new in the area. The findings are so far inconclusive regarding variable speed wind turbines [12]. However, the rationale of this study was to observe the impact of these two generators separately on the overall damping ratio of the system. This was done by replacing a synchronous generator in the IEEE 14 bus system and performing small signal stability analysis through PSAT. Later on generator frequency response was observed through time domain analysis in PSAT. PSSs for the synchronous generators were designed and a small disturbance was created to observe the improvement and impact in stability for both DFIG and DDSG integrated systems. In summary, the following conclusions can be drawn from this study:

1. WTGs have the capability to increase the small signal stability of a system if the synchronous generators participating towards oscillation is replaced by them. However, it can improve the damping only up to a certain level, depending on the wind penetration. Wind penetration has to be large enough to mitigate the oscillations

created by synchronous generators, and at the same time less enough to avoid weak grid issues. Other factors like placement of the WTG, inertia which have not been considered in this study might have significant impact as well.

2. For a certain level of penetration, DDSG integrated system has higher overall damping. As a result the oscillations are damped faster in DDSG than in DFIG integrated system. This holds true only when there is adequate q axis stator current for controlling rotor speed to generate the rated power. This varies with penetration, so under or above a certain penetration level, DDSG is no longer capable to provide the required damping in the system.

3. The maximum and minimum power delivered by the DDSG depend on the stator q axis current, which is largely dependent on the stator q axis reactance. On the other hand, DFIG is not as highly dependent on the reactance, allowing itself for a larger range of wind penetration.

4. The designed PSS increase the system damping. However, even if the damping ratios corresponding to electromechanical modes are higher in the case of DFIG, due to larger number of complex eigenvalues in DDSG after adding the PSSs, both the generator seem to damp out the oscillation at about the same time.

5. With the small disturbance occurring for different penetration levels, the time for the oscillations to damp out varies (80-100 s for DFIG and 60-80 s for DDSG) but with the PSSs, the oscillations damp out within 45-50 seconds of fault clearance for DFIG and within 40-45 seconds for DDSG, irrespective of the penetration level.

Recent works on DFIG show its integration is very likely to improve the stability of the system compared to the constant speed WTGs. It can also provide better small signal stability performance if replaced for a synchronous generator, because wind generators have no contribution to the system oscillations. On the other hand, the integration of DFIG and DDSG may reduce the damping of the system, if the marginal stability issue is not considered. This study, however finds the integration of variable speed WTG helpful in terms of damping out oscillations. The system was brought to asymptotically stable state from a marginally stable state and the damping ratios were improved using PSSs. This study also claims that wind penetration has a large role in deciding the overall damping of the system.

5.2 Future Work

Considering the limitations of this study, there are many potential fields to work on it in future; focusing on the placement of WTG, high penetration stability issues due to weak grid, impact of loss of inertia and fault location etc. Optimum placement of DFIG has been under research for quite sometime now, but DDSG integration is a whole new area to work on. Also, optimal and simultaneous placement of DFIG and DDSG in a system and their impact on stability would be a potential field to work on.

Again, further work can focus on higher wind penetration causing ”weak grid” issue. Solving this issue by increasing composite short circuit ratio (CSCR) through synchronous generators and condensers in the system is a current research interest that can be worked on.

On another note, the lack of power system dynamic analysis has been identified as a significant research gap from all of the large-scale regional wind and solar integration studies performed by he National Renewable Energy Laboratory (NREL) and others. Thus there is a need to analyze the dynamic behavior of a system under high variable renewable condition.

Another area to focus on, which has not been considered in this study is the inertia. Large penetration of generation technologies that are not synchronous further complicate this issue. Without special operation or controls, WTGs do not inherently participate in the regulation of grid frequency. By contrast, synchronous machines always contribute to system inertia. In fact, some fraction of the synchronous generation in operation at any point has governer controls enabled. Hence when wind generation displaces conventional synchronous generation, the mix of the remaining synchronous generators changes and has the potential to adversely impact overall frequency response. Therefore, the stability impact pf WTGs largely depend on inertia and this area of research needs further future attention.

In this study, only one location of fault or small disturbance has been considered. The location of fault being close to the WTG or far and it's impact on the stability is another area that can be worked on in future.

REFERENCES

[1] S.Heier. Grid integration of wind energy conversion systems. *Chichester,U. K. :Wiley*, 2006.

[2] U.S. Department of Energy. Wind Vision: A New Era for Wind Power in the United States. 2015.

[3] J. G.Slootweg. Wind power, modeling and impact on power system dynamics. *PhD Thesis, Power Systems Laboratory, Delft University of Technology*, 2003.

[4] P. Kundur. Power system stability and control. *New York: McGrawHill*, 1994.

[5] V. Aiiarapu P. Kundur, J. Paserba. Definition and classification of power system stability. *IEEE Trans. Power Syst., vol. 19, no. 3, pp. 1387-1401*, 2004.

[6] H.F.Wang W.Du and R.Dunn. Power system oscillation stability and control by facts and ESS-survey. *International Conference on Sustainable Power Generation and Supply, pp. 1-13*, 2009.

[7] Goran Andersson. Dynamics and Control of. Electric Power Systems. *Lecture 227-0528-00,ITET ETH, EEH - Power Systems Laboratory, ETH Zurich*, 2010.

[8] F. P. Demello and Concordia.C. Concepts of synchronous machine stability as affected by excitation control. *EEE Trans. Power Appar. & Syst., vol. PAS-88, no. 4, pp. 316-329*, 1969.

[9] F. J. Swift and H. F. Wang. The connection between modal analysis and electric torque analysis in studying the oscillation stability of multimachine power systems. *International Journal of Electrical Power and Energy Systems, vol. 19, no. 5, pp. 321-330*, 1997.

[10] Kliemann W Fouad A A. Chih-Ming Lin, Vittal V. Investigation of modal interaction and its effects on contral performace in stressed power systems using normal forms of vector fields. *IEEE Trans on Power Syst., vol. 11, no. 2, pp. 781-787*, 1996.

[11] C. J. Demeure J. F. Hauer and L. L. Scharf. Initial results in prony analysis of power system response signals. *IEEE Trans on Power Syst., vol. 5, no. 1, pp. 80-89, Feb*, 1990.

[12] W. Lixin S. Yuanzhang. A Review on Analysis and Control of Small Signal Stability of Power Systems with Large Scale Integration of Wind Power. *International Conference on Power System Technology*, 2010.

[13] M. Li H. F. Wang, F.J. Swift. A unified model for the analysis of FACTS devices in damping power system oscillations. II. Multimachine power systems . *IEEE Trans. Power Deliv. voU3, no. 4, pp. 1355-1362*, 1998.

[14] T. Smed and G. Andersson. Utilizing HVDC to damp power oscillations. *IEEE Trans. Power Deliv., vol. 8, no. 2, pp. 620-627*, 1993.

[15] Z. Zhiyi X. Yuxiao, Y. Rongxiang. Review of PSS based on W AMS suppressing low frequency oscillation of interconnected power grid. *Proceedings of the 2009 International Conference on Energy and Environment Technology , pp. 255-258*, 2009.

[16] H. Li and Z. Chen. Overview of different wind generator systems and their comparisons. *IET Renewable Power Generation, vol. 2, no. 2, pp. 123-138*, 2008.

[17] M. J. Gibbard D. J. Vowles, C. Samarasinghe. Effect of Wind Generation on Small-Signal Stability - A New Zealand Example. *2008 IEEE Power & Energy Society General Meeting, pp. 5217-5224*, 2008.

[18] V. Vittal D. Gautam and T. Harbour. Impact of increased penetration of DFIG-based wind turbine generators on transient and small signal stability of power systems. *IEEE Trans. Power Syst., vol. 24, no. 3, pp. 1426-1434*, Aug, 2009.

[19] N. Jenkins O. Anaya-Lara, F. M. Hughes. Influence of wind farms on power system dynamic and transient stability. *Wind Engineering, vol. 30, no. 2, pp. 107-27*, 2006.

[20] I. Norheim E. Hagstrom and K. Uhlen. Large-scale wind power integration in Norway and impact on damping in the Nordic grid. *Wind Energy, vol. 8, no. 3, pp. 375-384*, 2005.

[21] N. Jenkins F. M. Hughes, O. Anaya-Lara. A power system stabilizer for DFIG-based wind generation. *IEEE Trans. Power Syst.,vol. 21, no. 2, pp. 763-772*, 2006.

[22] B. Parsons E. Muljadi, C. P. Butterfield. Effect of variable speed wind turbine generator on stability of a weak grid. *IEEE Trans. on Energy Conversion, vol. 22, no. 1, pp. 29-36*, 2007.

[23] B. M. Nomikos G. Tsourakis and C. D. Voumas. Effect of wind parks with doubly fed asynchronous generators on small-signal stability. *Electric Power Systems Research, vol. 79, no. 1, pp. 190-200*, Jan, 2009.

[24] B. M. Nomikos G. Tsourakis and C. D. Voumas. Contribution of Doubly Fed Wind Generators to Oscillation Damping. *IEEE Trans. on Energy Conversion, vol. 24, no. 3, pp. 783-791*, Sep, 2009.

[25] N. R. Ullah and T. Thiringer. Effect of operational modes of a wind farm on the transient stability of nearby generators and on power oscillations: a Nordic grid study. *Wind Energy, vol. 11, no. 1, pp. 63-73*, 2008.

[26] M. Shao N.W. Miller. Western Wind and Solar Integration Study Phase 3 Frequency Response and Transient Stability. *Subcontract Report NREL/SR-5D00-62906*, December, 2014.

[27] A. B. Morton. Wind turbines and oscillatory stability in power systems: towards a general approach. *Proceedings of the 2009 Australasian Universities Power Engineering Conference (AUPEC 2009), pp. 6 pp.*, 2009.

[28] H. Guo B. Liu. Research on Small Signal Stability of Power System Connected with Different Wind Turbines Based on PSAT. *17th International Conference on Electrical Machines and Systems (ICEMS), Oct. 22-25*, 2014.

[29] Chang Yongjie. The Application of PSAT in Power System Stability Simulation. *Electrotechnical Journal 2008,pp.61-64*, 2008.

[30] F. Milano. Power System Analysis Toolbox: Documentation for PSAT. *version 1.3.4*, July 14, 2005.

[31] F. Milano. An open source power system analysis toolbox. *IEEE Trans. Power Syste., vol. 20, no.3*, Aug, 2005.

[32] B. Gao G.K. Morison and P. Kundur. Voltage stability analysis using static and dynamic approaches. *International Conference on Power System Technology*, Aug. 1993.

[33] P. W. Sauer and M. A. Pai. Power System Dynamics and Stability. *Upper Saddle River, NJ: Prentice-Hall*, 1998.

[34] M. S. Kumari D. R. Chandra. Small Signal Stability of Power System with SCIG, DFIG Wind Turbines. *Annual IEEE India Conference*, 2014.

APPENDIX A: POWER FLOW AND DYNAMIC DATA OF THE SYSTEM

This appendix depicts schemes and data of the 14-bus test system used in the study. Data are reported in the PSAT data format and were generated by the Simulink models provided with the toolbox.

With 5 synchronous generators:

```
Bus.con = [ ...
      1       69    1.06          0     4   1;
      2       69    1.045   -0.13577    4   1;
      3       69    1.01    -0.33247    4   1;
      4       69    0.99756 -0.26488    4   1;
      5       69    1.0029  -0.22667    4   1;
      6     13.8    1.07    -0.38565    2   1;
      7     13.8    1.0362  -0.34701    2   1;
      8       18    1.09    -0.34701    3   1;
      9     13.8    1.0134  -0.38858    2   1;
     10     13.8    1.0127  -0.39516    2   1;
     11     13.8    1.036   -0.39324    2   1;
     12     13.8    1.0461  -0.40624    2   1;
     13     13.8    1.0367  -0.40667    2   1;
     14     13.8    0.9973  -0.42256    2   1;
     ];
```

```
Line.con = [ ...
      2    5   100   69    60   0   0          0.05695   0.17388   0.034     0  0  0  0  0  1;
      6   12   100   13.8  60   0   0          0.12291   0.25581   0         0  0  0  0  0  1;
     12   13   100   13.8  60   0   0          0.22092   0.19988   0         0  0  0  0  0  1;
      6   13   100   13.8  60   0   0          0.06615   0.13027   0         0  0  0  0  0  1;
      6   11   100   13.8  60   0   0          0.09498   0.1989    0         0  0  0  0  0  1;
     11   10   100   13.8  60   0   0          0.08205   0.19207   0         0  0  0  0  0  1;
      9   10   100   13.8  60   0   0          0.03181   0.0845    0         0  0  0  0  0  1;
      9   14   100   13.8  60   0   0          0.12711   0.27038   0         0  0  0  0  0  1;
     14   13   100   13.8  60   0   0          0.17093   0.34802   0         0  0  0  0  0  1;
      7    9   100   13.8  60   0   0          0         0.11001   0         0  0  0  0  0  1;
      1    2   100   69    60   0   0          0.01938   0.05917   0.0528    0  0  0  0  0  1;
      3    2   100   69    60   0   0          0.04699   0.19797   0.0438    0  0  0  0  0  1;
      3    4   100   69    60   0   0          0.06701   0.17103   0.0346    0  0  0  0  0  1;
      1    5   100   69    60   0   0          0.05403   0.22304   0.0492    0  0  0  0  0  1;
      5    4   100   69    60   0   0          0.01335   0.04211   0.0128    0  0  0  0  0  1;
      2    4   100   69    60   0   0          0.05811   0.17632   0.0374    0  0  0  0  0  1;
      5    6   100   69    60   0   5          0         0.25202   0 0.932   0  0  0  0  0  1;
      4    7   100   69    60   0   5          0         0.20912   0 0.978   0  0  0  0  0  1;
      8    7   100   18    60   0   1.304348   0         0.17615   0         0  0  0  0  0  1;
     ];
```

```
Breaker.con = [ ...
       16        2   100   69   60   1   1   200;
       ];
```

```
SW.con = [ ...
    1      100   69    1.06    0     9.9     -9.9    1.2    0.8    2.324    1    1    1;
    ];

PV.con = [ ...
    3      100   69      1     1.045    0.5    -0.4    1.2   0.8   1   1;
    2      100   69     0.4    1.045    0.5    -0.4    1.2   0.8   1   1;
    6      100   13.8    0     1.07     0.24   -0.06   1.2   0.8   1   1;
    8      100   18      0     1.09     0.24   -0.06   1.2   0.8   1   1;
    ];

PQ.con = [ ...
    11     100   13.8   0.049    0.0252    1.2   0.8   0   1;
    13     100   13.8   0.189    0.0812    1.2   0.8   0   1;
    3      100   69     1.3188   0.266     1.2   0.8   0   1;
    5      100   69     0.1064   0.0224    1.2   0.8   0   1;
    2      100   69     0.3038   0.1778    1.2   0.8   0   1;
    6      100   13.8   0.1568   0.105     1.2   0.8   0   1;
    4      100   69     0.6692   0.056     1.2   0.8   0   1;
    14     100   13.8   0.2086   0.07      1.2   0.8   0   1;
    12     100   13.8   0.0854   0.0224    1.2   0.8   0   1;
    10     100   13.8   0.126    0.0812    1.2   0.8   0   1;
    9      100   13.8   0.413    0.2324    1.2   0.8   0   1;
    ];

Syn.con = [ ...
    1      615   69     60      3   0.24   0     0.9    0.3    0.23   7.4    0.03   0.65   0.64
    0.4    0     0.03   10.3    2   0      0     1      1      0      0      0      1      1;
    3      100   69     60      3   0      0.0   1.05   0.19   0.13   6.1    0.04   0.98   0.36
    0.13   0.3   0.1    13.08   2   0      0     1      1      0      0      0      1      1;
    2      60    69     60      3   0      0.0   1.05   0.19   0.13   6.1    0.04   0.98   0.36
    0.13   0.3   0.1    13.08   2   0      0     1      1      0      0      0      1      1;
    8      25    18     60      3   0.13   0.0   1.25   0.23   0.12   4.75   0.06   1.22   0.72
    0.12   1.5   0.21   10.12   2   0      0     1      1      0      0      0      1      1;
    6      25    13.8   60      3   0.13   0.0   1.25   0.23   0.12   4.75   0.06   1.22   0.71
    0.12   1.5   0.21   10.12   2   0      0     1      1      0      0      0      1      1;
    ];

Exc.con = [ ...
    1    2   7.32   0       100   0.02   0.002   1   1   0.2    0.001   0.0006   0.9   1;
    3    2   4.38   0       20    0.02   0.001   1   1   1.98   0.001   0.0006   0.9   1;
    2    2   4.38   0       20    0.02   0.001   1   1   1.98   0.001   0.0006   0.9   1;
    4    2   6.81   1.395   20    0.02   0.001   1   1   0.7    0.001   0.0006   0.9   1;
    5    2   6.81   1.395   20    0.02   0.001   1   1   0.7    0.001   0.0006   0.9   1;
    ];

Bus.names = {...
  'Bus 01';    'Bus 02';   'Bus 03';   'Bus 04';   'Bus 05';
  'Bus 06';    'Bus 07';   'Bus 08';   'Bus 09';   'Bus 10';
  'Bus 11';    'Bus 12';   'Bus 13';   'Bus 14'};

Dfig.con = [ ...
    3     1    100    69   60   0.01   0.1          0.01   0.08   3     3      10
    3     10   0.01   62   4    3      0.01123596   1      0      0.7   -0.7   20   1;
    ];

Ddsg.con = [ ...
    3     1      100    69   60   0.01   0.01         0.08   1   3     10     3    10
    1     0.01   0.01   62   4    3      0.01123596   1      0   0.7   -0.7   20   1;
    ];

Wind.con = [ ...
    3     15   1.225   4   0.1   20   2   5   15   0   5   15   0   50   0   0.2   50   10   1;
    ];
```

APPENDIX B: CODES FOR DESIGNING POWER SYSTEM STABILIZER

PSS Design for DFIG Integrated System:

Code for Gen 2 PSS:

```
a11=-0.19425;a12=-0.0306;a13=-0.06187;a14=0;

a21=376.9911;

a22=0;a23=0;a24=0;a31=0;a34=0;a41=0;

a32=-0.01796;a33=-0.18691;

a42=-27.2066;a43=814.6482;a44=-1000;

Ld=1.05; Ldd=0.185; Ll=0;

H=6.54;

Lad=Ld-Ll;

Lfd=(Lad*Ldd-Ll*Lad)/(Lad-Ldd+Ll)

Tdd=6.1;

Ka=20;

s=0.06424+7.9349i;

Rfd=(Ld+Lfd)/(Tdd*a21)

Tr=-(1/a44)

T3=-(1/a33)

Kd=-2*H*a11

K1=-2*H*a12

K2=-2*H*a13

b11=1/(2*H)

b32=(a21*Rfd)/Ld

K3=-(b32/a33)

K4=-(a32/b32)

K5=a42*Tr

K6=a43*Tr

neu=-K2*K3*(K4*(1+s*Tr)+K5*Ka)

deno=s*s*T3*Tr+s*(T3+Tr)+1+K3*K6*Ka
```

$delta_T e$=(neu/deno)

```
Tpss=K2*(K3*Ka)/(s*T3+1+K3*K6*Ka)
```

Results:

Lfd = 0.2246

Rfd = 5.5424e-04

Tr = 1.0000e-03

T3 = 5.3502

Kd =2.5408

K1 = 0.4002

K2 =0.8093

b11 = 0.0765

b32 = 0.1990

K3 =1.0647

K4 =0.0903

K5 = -0.0272

K6 = 0.8146

neu = 0.3911 - 0.0006i

deno =18.3534 +42.4664i

$delta_T e$ =0.0033 - 0.0078i

Tpss =0.1497 - 0.3400i

Code for Gen 3 PSS:

```
a11=-0.19425;a12=-0.0306;a13=-0.06187;a14=0;

a21=376.9911;

a22=0;a23=0;a24=0;a31=0;a34=0;a41=0;

a32=-0.01796;a33=-0.18691;

a42=-27.2066;a43=814.6482;a44=-1000;

Ld=1.25; Ldd=0.232; Ll=0.134;

H=5.06;

Lad=Ld-Ll;

Lfd=(Lad*Ldd-Ll*Lad)/(Lad-Ldd+Ll)

Tdd=4.75;

Ka=20;

s=0.11414+8.26509i;

Rfd=(Ld+Lfd)/(Tdd*a21)

Tr=-(1/a44)

T3=-(1/a33)

Kd=-2*H*a11

K1=-2*H*a12
```

K2=-2*H*a13

b11=1/(2*H)

b32=(a21*Rfd)/Ld

K3=-(b32/a33)

K4=-(a32/b32)

K5=a42*Tr

K6=a43*Tr

neu=-K2*K3*(K4*(1+s*Tr)+K5*Ka)

deno=s*s*T3*Tr+s*(T3+Tr)+1+K3*K6*Ka

$delta_T e$=(neu/deno)

Tpss=K2*(K3*Ka)/(s*T3+1+K3*K6*Ka)

Results:

Lfd =0.1074

Rfd =7.5804e-04

Tr =1.0000e-03

T3 =5.3502

Kd = 1.9658

K1 = 0.3097

K2 = 0.6261

b11 =0.0988

b32 =0.2286

K3 =1.2232

K4 = 0.0786

K5 = -0.0272

K6 = 0.8146

neu = 0.3566 - 0.0005i

deno = 21.1742 +44.2380i

$delta_T e$ = 0.0031 - 0.0066i

Tpss = 0.1364 - 0.2800i

Code for Gen 4 PSS:

a11=-0.19425;a12=-0.0306;a13=-0.06187;a14=0;

a21=376.9911;

a22=0;a23=0;a24=0;a31=0;a34=0;a41=0;

a32=-0.01796;a33=-0.18691;

```
a42=-27.2066;a43=814.6482;a44=-1000;

Ld=1.25; Ldd=0.232;Ll=0.134;

H=5.06;

Lad=Ld-Ll;

Lfd=(Lad*Ldd-Ll*Lad)/(Lad-Ldd+Ll)

Tdd=4.75;

Ka=20;

s=-0.09709+9.14269i;

Rfd=(Ld+Lfd)/(Tdd*a21)

Tr=-(1/a44)

T3=-(1/a33)

Kd=-2*H*a11

K1=-2*H*a12

K2=-2*H*a13

b11=1/(2*H)

b32=(a21*Rfd)/Ld

K3=-(b32/a33)

K4=-(a32/b32)

K5=a42*Tr

K6=a43*Tr

neu=-K2*K3*(K4*(1+s*Tr)+K5*Ka)

deno=s*s*T3*Tr+s*(T3+Tr)+1+K3*K6*Ka
```

$delta_T e$=(neu/deno)

```
Tpss=K2*(K3*Ka)/(s*T3+1+K3*K6*Ka)
```

Results:

Lfd = 0.1074

Rfd =7.5804e-04

Tr =1.0000e-03

T3 = 5.3502

Kd = 1.9658

K1 = 0.3097

K2 =0.6261

b11 = 0.0988

b32 =0.2286

K3 =1.2232

K4 =0.0786

K5 =-0.0272

K6 = 0.8146

neu =0.3566 - 0.0006i

deno =19.9622 +48.9146i

$delta_T e$=0.0025 - 0.0063i

Tpss =0.1113 - 0.2667i

PSS Design for DDSG Integrated System:

Code for GEN 2 PSS:

```
a11=-0.19763;a12=-0.17784;a13=-0.01591;a14=0;

a21=376.9911;

a22=0;a23=0;a24=0;a31=0;a34=0;a41=0;

a32=0.020066;a33=-0.86508;

a42=17.03581;a43=291.0661;a44=-1000;

Ld=1.05; Ldd=0.1850, Ll=0;

H=6.54;

Lad=Ld-Ll;

Lfd=(Lad*Ldd-Ll*Lad)/(Lad-Ldd+Ll)

Tdd=6.1;

Ka=20;

s=-0.05835+7.93249i;

Rfd=(Lad+Lfd)/(Tdd*a21)

Tr=-(1/a44)

T3=-(1/a33)

Kd=-2*H*a11

K1=-2*H*a12

K2=-2*H*a13

b11=1/(2*H)

b32=(a21*Rfd)/Ld

K3=-(b32/a33)

K4=-(a32/b32)

K5=a42*Tr

K6=a43*Tr
```

neu=-K2*K3*(K4*(1+s*Tr)+K5*Ka)

deno=s*s*T3*Tr+s*(T3+Tr)+1+K3*K6*Ka

$delta_Te$=(neu/deno)

Tpss=K2*(K3*Ka)/(s*T3+1+K3*K6*Ka)

Results:

Ldd =0.1850

Lfd =0.2246

Rfd =5.5424e-04

Tr =1.0000e-03

T3 =1.1560

Kd =2.5850

K1 =2.3261

K2 =0.2081

b11 =0.0765

b32 =0.1990

K3 =0.2300

K4 =-0.1008

K5 =0.0170

K6 =0.2911

neu =-0.0115 + 0.0000i

deno =2.1988 + 9.1765i

$delta_Te$ =-0.0003 + 0.0012i

Tpss =0.0244 - 0.0984i

Code for GEN 3 PSS:

a11=-0.19763;a12=-0.17784;a13=-0.01591;a14=0;

a21=376.9911;

a22=0;a23=0;a24=0;a31=0;a34=0;a41=0;

a32=0.020066;a33=-0.86508;

a42=17.03581;a43=291.0661;a44=-1000;

Ld=1.25; Ldd=0.232, Ll=0.134;

H=5.06;

Lad=Ld-Ll;

Lfd=(Lad*Ldd-Ll*Lad)/(Lad-Ldd+Ll)

Tdd=4.75;

Ka=20;

s=-0.11477+8.26566i;

Rfd=(Lad+Lfd)/(Tdd*a21)

Tr=-(1/a44)

T3=-(1/a33)

Kd=-2*H*a11

K1=-2*H*a12

K2=-2*H*a13

b11=1/(2*H)

b32=(a21*Rfd)/Ld

K3=-(b32/a33)

K4=-(a32/b32)

K5=a42*Tr

K6=a43*Tr

neu=-K2*K3*(K4*(1+s*Tr)+K5*Ka)

deno=s*s*T3*Tr+s*(T3+Tr)+1+K3*K6*Ka

$delta_T e$=(neu/deno)

Tpss=K2*(K3*Ka)/(s*T3+1+K3*K6*Ka)

Results:

Ldd =0.2320

Lfd =0.1074

Rfd =6.8321e-04

Tr =1.0000e-03

T3 =1.1560

Kd =2.0000

K1 =1.7997

K2 =0.1610

b11 =0.0988

b32 =0.2061

K3 =0.2382

K4 =-0.0974

K5 =0.0170

K6 =0.2911

neu =-0.0093 + 0.0000i

deno =2.1748 + 9.5609i

$delta_T e$=-2.0804e-04 + 9.2878e-04i

Tpss =0.0179 - 0.0760i

Code for GEN 4 PSS:

```
a11=-0.19763;a12=-0.17784;a13=-0.01591;a14=0;
a21=376.9911;
a22=0;a23=0;a24=0;a31=0;a34=0;a41=0;
a32=0.020066;a33=-0.86508;
a42=17.03581;a43=291.0661;a44=-1000;
Ld=1.25; Ldd=0.232, Ll=0.134;
H=5.06;
Lad=Ld-Ll;
Lfd=(Lad*Ldd-Ll*Lad)/(Lad-Ldd+Ll)
Tdd=4.75;
Ka=20;
s=-0.11477+8.26566i;
Rfd=(Lad+Lfd)/(Tdd*a21)
Tr=-(1/a44)
T3=-(1/a33)
Kd=-2*H*a11
K1=-2*H*a12
K2=-2*H*a13
b11=1/(2*H)
b32=(a21*Rfd)/Ld
K3=-(b32/a33)
K4=-(a32/b32)
K5=a42*Tr
K6=a43*Tr
neu=-K2*K3*(K4*(1+s*Tr)+K5*Ka)
deno=s*s*T3*Tr+s*(T3+Tr)+1+K3*K6*Ka
```

$delta_T e$=(neu/deno)

```
Tpss=K2*(K3*Ka)/(s*T3+1+K3*K6*Ka)
```

Results:

Ldd = 0.2320

Lfd =0.1074

Rfd =6.8321e-04

Tr =1.0000e-03

T3 = 1.1560

Kd = 2.0000

K1 = 1.7997

K2 =0.1610

b11 =0.0988

b32 = 0.2061

K3 =0.2382

K4 =-0.0974

K5 =0.0170

K6 = 0.2911

neu = -0.0093 + 0.0000i

deno = 2.1770 +10.5754i

$delta_T e$= -1.7117e-04 + 8.4721e-04i

Tpss = 0.0149 - 0.0694i